[American Journal of Science, Vol. 314, May, 2014, P. 895–939, DOI 10.2475/05.2014.01]

American Journal of Science

MAY 2014

EVOLUTION OF MAJOR AND TRACE ELEMENT COMPOSITION DURING MELT MIGRATION THROUGH CRYSTALLINE MUSH: IMPLICATIONS FOR CHEMICAL DIFFERENTIATION IN THE CRUST

J. M. S. SOLANO*,**, M. D. JACKSON*,†, R. S. J. SPARKS***, and J. BLUNDY***

ABSTRACT. We present the first quantitative model of heat, mass and both major and trace element transport in a mush undergoing compaction that accounts for component transport and chemical reaction during melt migration and which is applicable to crustal systems. The model describes the phase behavior of binary systems (both eutectic and solid solution), with melt and solid compositions determined from phase diagrams using the local temperature and bulk composition. Trace element concentration is also determined. The results demonstrate that component transport and chemical reaction generate compositional variation in both major and trace elements that is not captured by existing geochemical models. In particular, we find that, even for the simplest case of a homogenous, insulated column that is instantaneously melted then allowed to compact, component transport and reaction leads to spatial variations in major element composition that, in this case, produces melt that is more enriched in incompatible elements than predicted by batch melting. In deep crustal hot zones (DCHZ), created by the repeated intrusion of hot, mantle-derived magmas, buoyant melt migrating upwards accumulates in high porosity layers, but has a composition corresponding to only a small fraction of batch melting, because it has locally equilibrated with mush at low temperature; moreover, melt migration and chemical reaction in a layered protolith may lead to the rapid formation of high porosity melt layers at the interface between different rock compositions. In both of these cases, the melt in the high porosity layer(s) is less enriched in incompatible trace elements than predicted if it is assumed that melt with the same major element composition was produced by batch melting. This distinctive decoupling of major and trace element fractionation may be characteristic of magmas that originate in DCHZ. Application of the model to a number of crustal systems, including the Ivrea-Verbano zone, the Rum layered intrusion, and the Holyoke flood basalt, suggests that compositional heterogeneity can be explained by buoyancy-driven melt migration and component transport through a reactive crystalline mush.

INTRODUCTION

Migration of melt through crystal mush is a common process within the Earth's crust. Mush formation is inevitable during melting of solid rock or crystallization of magma. When the melt content of the mush is above a threshold value (typically $<2\%$) it forms an interconnected network along grain boundaries, so the matrix is permeable (von Bargen and Waff, 1986; Wolf and Wyllie, 1991; Petford, 2003; Rosenberg and Handy, 2005). A pressure gradient is also normally present, because the melt is compositionally buoyant, which causes melt flow relative to the crystalline matrix

* Department of Earth Science and Engineering, Imperial College, London, SW7 2AZ, United Kingdom
** Brevan Howard, 55 Baker Street, London, W1U 8EW, United Kingdom
*** School of Earth Sciences, University of Bristol, Wills Memorial Building, Queens Road, Bristol BS8 1RJ, United Kingdom
† Corresponding author: m.d.jackson@imperial.ac.uk

(McKenzie, 1984). The matrix can deform in response to melt flow via melt-enhanced creep (Dell'Angelo and others, 1987; Mei and others, 2002); the coupled process of melt migration and matrix deformation is termed compaction (McKenzie, 1984). There is abundant evidence that melt migration via compaction is a fundamental process of melt-solid segregation and occurs in a wide variety of crustal igneous systems (Wager, 1961; Irvine, 1974; Wilson and others, 1981; Sparks and others, 1985; Shirley, 1986; Tharp and others, 1998; Boudreau and Philpotts, 2002; Bachmann and Bergantz, 2004; Hersum and others, 2007; Tegner and others, 2009).

In the middle and lower crust, segregation of evolved melt from crystal mush has been invoked to explain the origin of silicic (granitic *sensu-lato*) magmas. In this setting, the intrusion of hot, mantle-derived basaltic magmas into crustal rocks generates a region of crystal mush, in which the melt phase originates both from crystallization of the basalt, and partial melting of the crust. The buoyant melt migrates along grain boundaries and accumulates until it forms a mobile magma that can leave the source region and ascend to shallower crustal levels (for example, Jackson and others, 2003, 2005; Solano and others, 2012). In the upper crust, magmas ascending from depth can accumulate in shallow crustal reservoirs that typically grow incrementally (for example, Coleman and others, 2004; Annen, 2009). The combined processes of heat advection through repeated inputs of magma, heat loss through the wall and roof rocks, and degassing (in the case of volatile-bearing magmas), leads to both crystallization and partial melting, and the formation of crystal mushes in these "active plutons" (Claiborne and others, 2010; Cashman and Blundy, 2013). Active plutons may solidify *in-situ*, or give rise to volcanic eruptions if the melt can escape. In either case, mush processes play an important role in redistributing and accumulating melts. Melt migration through a crystal mush has been invoked to explain some of the observed compositional variation in magmas that leave the chamber and in the crystal cumulates that are preserved *in-situ* (Irvine, 1980; Naslund and McBirney, 1996 and references therein; Holness, 2005; Holness and others, 2007; Holness and Winpenny, 2008). At or close to the Earth's surface, crystal mushes can form as a result of cooling of magma in sills and lava flows. Here, melt migration has been invoked to explain characteristic compositional profiles from the outer contacts to the interior (for example, Philpotts and others, 1996; Boudreau and Philpotts, 2002; Latypov, 2003 and references therein).

Melt migration through a crystal mush is an example of coupled phase change and phase transport within a complex, multi-component substance. When melt migration occurs along grain boundaries, there is efficient exchange of heat and mass between melt and solid phases, so they remain in local thermal and chemical equilibrium (Jackson and others, 2005). The composition of the melt therefore evolves as it migrates through the mush and, to properly capture this, models are required that include component transport and chemical reaction (for example, Oertling and Watts, 2004; Le Bars and Worster, 2006; Katz and Worster, 2008). In the geological literature, most studies have focused on mantle processes; in particular the generation and segregation of melt during adiabatic upwelling below mid-ocean ridges. Ribe (1985) presented a model for both eutectic and solid solution binary systems undergoing adiabatic decompression. Sparks and Parmentier (1991) showed compaction was required to focus magma under cold lithosphere, whilst Spiegelman (1993, 1996) modeled isotopic variation during compaction, assuming melting is coupled to the upwelling rate but neglecting freezing. Melting of a single component mantle during adiabatic upwelling has been modeled by Šrámek and others (2007) and Hewitt and Fowler (2008), including phase change, interfacial stresses and an explicit description of phase pressure differences. Katz (2008) presented an enthalpy-based approach to describe phase changes in upwelling mantle, in which melt migration with component

transport and chemical reaction was explicitly included, using a binary solid-solution phase diagram with pressure-dependent liquidus and solidus temperatures.

Models of melting and melt migration in the crust have not included component transport and chemical reaction. Most consider either heat transfer and associated phase change but neglect melt migration (Hodge, 1974; Bergantz 1989; Petford and Gallagher, 2001; Annen and Sparks, 2002; Dufek and Bergantz, 2005; Annen and others, 2006; Annen, 2009), or migration of a pre-existing melt fraction with no further phase change or chemical reaction (McKenzie, 1984; Richter and McKenzie, 1985; Sparks and others, 1985; Scott and Stevenson, 1986; Vasilyev and others, 1998). In models of heat transfer, the melt fraction and chemical composition of the melt for a given initial bulk rock composition, temperature and pressure, are specified using parameterized data from laboratory experiments. A small number of coupled models of heat and mass transfer have been presented, but these use the same parameterized data to describe phase change and melt composition as models that neglect melt migration (Fountain and others, 1989; Jackson and Cheadle, 1998; Jackson and others, 2003, 2005; Solano and others, 2012). The problem with this approach is that melt migration changes the local bulk composition (that is, the melt + solid composition at a specific location), which invalidates the use of parameterized data obtained for a single bulk composition. This was recognized by Rushmer and Jackson (2008), who presented a revised experimental approach that attempts to account for changes in bulk composition during melt migration. Their approach was applied by Getsinger and others (2009), who observed that melt migration and chemical reaction lead to significant variations in melt composition that are not captured by the commonly applied batch or fractional melting models.

Phase compositions during phase change in the crust have been described using programs such as MELTS (Ghiorso and Sack, 1995; Asimow and Ghiorso, 1998); for example, Gutierrez and Parada (2010) used MELTS to investigate compositional variation in a convecting magma chamber, while Boudreau and Philpotts (2002) modeled compaction in a cooling basalt lava flow. However, neither of these studies explicitly modeled component transport; moreover, phase equilibration was ignored at melt fractions below 10 percent, a regime in which compaction is important. A fully coupled model of melt migration through a crystal mush within the crust, which accounts for phase change, component transport, chemical reaction and compaction, has not yet been developed. Coupled models of heat and mass transfer, which include component transport, chemical reaction and compaction, but which have been developed to describe melting in the mantle, are not directly applicable to crustal igneous systems because the initial and boundary conditions are different. Most significantly, mantle models consider melting due to adiabatic upwelling, whereas phase change in the crust typically results from the addition or removal of heat. There is a need for a model of compaction coupled to component transport and chemical reaction that can be applied to crustal magmatic systems. Such models should include explicitly the behavior of trace elements, as these are important tools when modeling magma genesis. Fractionation of trace elements provides insights into the processes that lead to chemical differentiation.

A number of trace element models have been developed which fall into four main categories: batch models, fractional models (for example, Schilling and Winchester, 1969; Shaw, 1970), continuous models (for example, Zou, 1998, 2000; Williams and Gill, 1989; Albarède, 1996) and dynamic models (for example, Langmuir and others, 1977; McKenzie, 1985; Ribe, 1985; Reiners, 1998). Batch, fractional and continuous models consider only phase change, whereas dynamic models also consider melt migration. Phase change has been coupled to melt migration and trace element transport in models applied to melt generation in the mantle during adiabatic

upwelling (Richter, 1986; Navon and Stolper, 1987; Spiegelman, 1996; Zou, 1998; Reiners, 1998; Shaw, 2000). Trace element variation has also been modeled in crustal systems, where assimilation of crustal material may be important. These models include assimilation-fractional crystallization (AFC; De Paolo, 1981), energy-constrained recharge assimilation and fractional crystallization (EC-RAFC; Spera and Bohrson, 2001) and melting-assimilation-storage-hybridisation (MASH; Hildreth and Moorbath, 1988). However, despite this plethora of models to describe trace element behavior in igneous systems, it is unclear which, if any, are able to capture the behavior of trace elements in crystal mushes where compaction-driven melt migration and consequent melt-crystal chemical reactions play an important role (for example, Spiegelman, 1996).

The aim of this paper is to develop a coupled model of heat and mass transfer within a partially molten crystal mush, which includes major and trace element transport, chemical reaction and compaction, and which is applicable to crustal igneous systems. We use the enthalpy method to describe conservation of heat, and simple phase diagrams to describe solid and melt compositions, in an approach similar to that presented for the mantle by Katz (2008). The formulation of McKenzie (1984) is followed to model compaction. Phase changes and compositions are described using simple binary eutectic (for example, Diopside-Forsterite, Anorthite-Diopside, Orthoclase-Quartz) and solid solution (for example, Forsterite-Fayalite, Albite-Anorthite) phase diagrams that approximate the behavior of natural systems. Trace element partitioning between crystals and melts is included. Our simplified approach to phase equilibria is chosen in preference to a more complex approach involving, for example, MELTS (Ghiorso and Sack, 1995; Asimow and Ghiorso, 1998) for three reasons: first, component transfer leads to local changes in bulk composition, so the local phase equilibria must be recalculated at each location and time; this is trivial using a simple phase diagram, but computationally intensive using a program such as MELTS. Second, we wish to elucidate the fundamental aspects of compositional evolution during compaction of igneous mushes without the additional complexity associated with modeling the phase behavior of natural systems. Finally, our simple one-dimension (1-D) model approach could be reproduced, at least in principle, in laboratory experiments (for example, Walte and others, 2005). We omit differential stresses imposed by tectonic forces, magma chamber over-pressuring, loading and other mechanisms (see, for example, Karlstrom and others, 2009, 2010), noting that melt segregation in mushes always requires at least some grain-boundary flow and buoyancy is always present to drive this. Moreover, while we recognize that compaction is not the only segregation mechanism that may operate in partially molten igneous systems, there is abundant evidence that compaction occurs in a variety of settings within the continental crust (for example Wager, 1961; Irvine, 1974; Wilson and others, 1981; Shirley, 1986; Boudreau and Philpotts, 2002; Bachmann and Bergantz, 2004; Hersum and others, 2007; Tegner and others, 2009) and, as yet, no other quantitative models have been presented that can predict temperature, melt fraction and melt transport rates in crustal mushes. We argue that our approach is a reasonable first step, and that a physico-chemical model that captures at least some of the key physics of melt segregation, provides useful insight which cannot be obtained from purely chemical models that omit segregation entirely. We apply the model to a number of natural crustal igneous systems, including the Mafic Complex of the Ivrea-Verbano zone in Italy, the so-called "Wavy Horizon" of the Rum layered intrusion in Scotland, and the Holyoke Flood Basalt in the USA, and demonstrate that it predicts—to first order—observed variations in major and trace element composition.

MODEL FORMULATION

The transport of heat, mass and components is modeled in 1-D, using a continuum formulation of the governing conservation equations in a deformable mush undergoing buoyancy-driven melt migration along grain boundaries. The system is assumed to be in local thermodynamic equilibrium, because the Péclet number, estimated using diffusion coefficients measured on a range of common crustal minerals (for example, Freer, 1981) and a reasonable range of Darcy flow rates, is $\ll 1$ (Jackson and others, 2005). The melt phase is interconnected and buoyant; the solid phase is able to deform viscously. The Boussinesq approximation is applied, so density differences between solid and liquid are neglected except for terms involving gravity. Energy conservation is solved using the enthalpy method (Shamsundar and Sparrow, 1975; Schneider and Beckerman, 1991; with application to mantle melting by Katz, 2008). Surface tension, interphase pressure, and grain damage (that is, the development of micro-cracks and defects within the crystals) are neglected, in common with numerous previous studies (for example, McKenzie, 1984, 2011; Spiegelman, 1993, 1996; Jackson and others, 2003; Katz, 2008; Solano and others, 2012); work has begun to extend the compaction model to include these potentially important effects, but a single, self-consistent formulation that also includes phase change has not yet been presented (see, for example, Bercovici and others, 2001; Ricard and others, 2001; Bercovici and Ricard, 2003; Šrámek and others, 2007; Simpson and others, 2010; Khazan, 2010). Momentum conservation equations follow the formulation of McKenzie (1984), with the addition of melt fraction-dependent solid viscosity (Connolly and Podladchikov, 1998). The component transport equations are based on the continuum formulation of Bennon and Incropera (1987), and the approach of Katz (2008) is used to determine melt fraction. Note that melt fraction and porosity are synonymous in this model. However, the change in local bulk composition that results from melt migration means that the melt fraction considered here cannot be simply related to a melt fraction calculated relative to the initial bulk composition, as is commonly used in the trace element models listed above.

The model represents a cylindrical column that can be perfectly insulated on all sides (fig. 1). Initially, we assume that a compositionally homogenous, solid column is instantaneously brought to a constant temperature above the solidus and then allowed to compact; this configuration has been investigated in previous studies (for example, McKenzie, 1984; Richter and McKenzie, 1985; Scott and Stevenson, 1986; Vasilyev and others, 1998) and here we explore the impact of chemical reaction on melt fraction and temperature (fig. 1A). We then investigate the same initial condition in a compositionally heterogeneous, solid column, where mixing of melts sourced from different solid compositions occurs as a result of melt migration (fig. 1B). Next we investigate heating of initially homogenous (fig. 1C) and heterogeneous (fig. 1D) solid columns from below, to mimic melt generation in deep crustal hot zones (for example, Petford and Gallagher, 2001; Annen and Sparks, 2002; Jackson and others, 2003, 2005; Annen and others, 2006; Solano and others, 2012), and in the cumulate pile within some layered intrusions (for example, Holness and others, 2007) (fig. 1B). Finally, we model cooling of an initially homogenous and partially molten column from above and below, to mimic melt segregation in sills and lava flows (for example, Philpotts and others, 1996; Boudreau and Philpotts, 2002; Latypov, 2003) (fig. 1E).

Governing Equations

Conservation of energy is defined using an enthalpy formulation and is given by (see table 1 for the Nomenclature)

$$\frac{\partial h}{\partial t} = \frac{k_T}{\rho}\frac{\partial^2 T}{\partial z^2} + L_f \frac{\partial}{\partial z}((1-\phi)w_S). \tag{1}$$

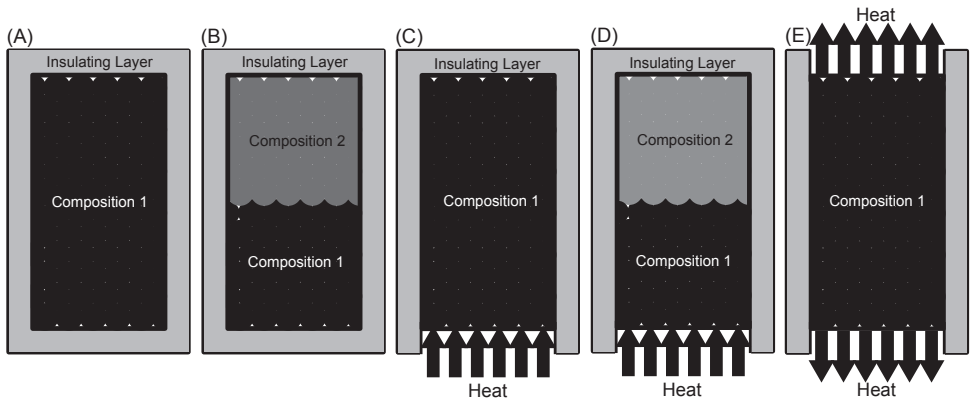

Fig. 1. The models investigated here represent an initially solid column with either (A) constant composition, brought instantaneously to a temperature above the solidus and then allowed to compact, with no further heat entering or leaving the column, (B) two layers of contrasting composition, brought instantaneously to a temperature above the solidus and then allowed to compact, with no further heat entering or leaving the column, (C) constant composition, heated from below to a temperature above the solidus and allowed to compact, (D) two layers of contrasting composition, heated from below to a temperature above the solidus and allowed to compact, or (E) constant composition, brought instantaneously to a temperature above the solidus and then allowed to compact, with cooling from above and below. In all cases, no flow is allowed across the column boundaries.

Conservation of major elements, neglecting diffusion, is given by

$$\frac{\partial C}{\partial t} = -\frac{\partial}{\partial z}\left((1-\phi)w_S C_S\right) - \frac{\partial}{\partial z}\left(\phi w_L C_L\right) \tag{2}$$

while conservation of trace elements, again neglecting diffusion, is given by

$$\frac{\partial I}{\partial t} = -\frac{\partial}{\partial z}\left((1-\phi)w_S I_S\right) - \frac{\partial}{\partial z}\left(\phi w_L I_L\right). \tag{3}$$

We neglect mass diffusion, given the small Péclet number. Conservation of momentum is given by

$$\eta_0 \frac{\partial}{\partial z}\left(\phi^{-\beta}\frac{\partial w_S}{\partial z}\right) = \frac{\mu w_S}{k_\phi} + (1-\phi)\Delta\rho g \tag{4}$$

where the melt fraction dependent viscosity is defined as

$$\frac{4}{3}\eta + \zeta = \eta_0 \phi^{-\beta}. \tag{5}$$

The permeability is given by

$$k_\phi = a^2 b \phi^\alpha. \tag{6}$$

Melt fraction is related to composition for the binary phase diagrams considered here through

$$\phi = \frac{C - C_S}{C_L - C_S} \tag{7}$$

TABLE 1

Nomenclature

Symbol	Description	Unit
a	grain radius	m
b	permeability constant	none
c_p	specific heat capacity	$J \cdot kg^{-1} \cdot K^{-1}$
C	local bulk composition	none
C_L	melt (liquid) composition	none
C_S	solid composition	none
C_i	initial bulk composition	none
e	eutectic composition	none
g	acceleration due to gravity	ms^{-2}
h	enthalpy	J
h_S	solidus enthalpy	J
h_L	liquidus enthalpy	J
I	local bulk concentration	none
I_S	solid concentration	none
I_L	melt concentration	none
I_i	initial concentration	none
k_T	thermal conductivity	$W \cdot K^{-1} \cdot m^{-1}$
k_ϕ	permeability	m^{-2}
K_ϕ	characteristic permeability scale	m^{-2}
K	partition coefficient	none
L_f	latent heat of fusion	$J \cdot kg^{-1}$
P_S	weighted solid contribution	none
P_L	weighted melt contribution	none
Ste	Stefan number	none
t	time	s
T	temperature	K
T_{geo}	geothermal gradient	$K \cdot m^{-1}$
T_S	solidus temperature	K
T_L	liquidus temperature	K
T_i	initial temperature	K
w_S	matrix velocity	ms^{-1}
w_L	melt velocity	ms^{-1}
z	vertical coordinate	M
z_M	top of mush	M
z_{Mi}	top of column (initial top of mush)	M
α	permeability exponent	None
β	viscosity exponent	None
δ	characteristic length scale	M
ϕ	porosity (≡ melt fraction)	None
ϕ_i	initial porosity	None
η	matrix bulk viscosity	$Pa \cdot s$
η_0	effective matrix viscosity	$Pa \cdot s$
μ	melt shear viscosity	$Pa \cdot s$
ξ	matrix shear viscosity	$Pa \cdot s$
ρ	density	$Kg \cdot m^{-3}$
ρ	solid-melt density difference	$Kg \cdot m^{-3}$
τ	characteristic time scale	s
ω	characteristic velocity scale	ms^{-1}

where C is the local bulk composition; note that the initial bulk composition (C_i) does not feature in this formulation of melt fraction.

Assuming a linear release of enthalpy during melting, enthalpy is related to temperature through

$$h = c_P T + L_f \phi. \tag{8}$$

Using equations (7) and (8), and the temperature-dependent liquid and solid compositions determined from the phase diagram (discussed in the next section), the melt fraction can be determined locally without the need to solve explicitly for mass conservation. For non-modal melting, the concentration of a trace element in the melt is given by (Shaw, 1970)

$$I_L = \frac{I}{P_S + \phi(1 - P_L)} \tag{9}$$

and in the solid by

$$I_S = \frac{I(P_S - \phi P_L)}{(1 - \phi)(P_S + \phi(1 - P_L))} \tag{10}$$

where I is the local bulk composition. The weighted average of the solid contribution to the partition coefficient is given by

$$P_S = (1 - \phi) \sum_j C_{Sj} K_{j-m} \tag{11}$$

where K_{j-m} is the Nernst partition coefficient between component j and the melt for each solid phase. The weighted average of the melt contribution is given by

$$P_L = \phi \sum_j C_{Lj} K_{j-m}. \tag{12}$$

Elements with $K < 1$ are incompatible and readily enter the melt; elements with $K > 1$ are compatible and remain in the solid phase. Note that equations (9) and (10) are usually expressed in terms of the mass fraction (F); here, F and ϕ are equivalent because we invoke the Boussinesq approximation, in which density variations are neglected except in terms that include gravity. Note also that F is calculated using the *local* bulk composition, which changes in response to melt migration.

Phase Behavior of Binary Systems

The phase diagrams modeled are the Anorthite-Diopside eutectic and the Albite-Anorthite solid solution systems (fig. 2). These are representative of common rock-forming minerals, and were chosen as examples of binary eutectic and solid solutions that are geologically relevant (for example, Bowen, 1928; Weill and others, 1980). The results we obtain illustrate principles, which also apply to more complex, multi-component systems; they differ quantitatively if other phase diagrams are used, but the general behavior and conclusions remain the same. In both cases, the composition-temperature relationships, C–T, have been derived by fitting a quadratic equation to the experimental data of Weill and others (1980). The binary eutectic is described by

$$C_L = \begin{cases} \dfrac{-b_1 - \sqrt{b_1^2 - 4a_1(c_1 - T)}}{2a_1} & C < e \\ \dfrac{-b_2 + \sqrt{b_2^2 - 4a_2(c_2 - T)}}{2a_2} & C > e \end{cases} \tag{13}$$

$$C_S = \begin{cases} 0, C < e \\ 1, C > e \end{cases} \tag{14}$$

$$a_1 = -466, \quad b_1 = -135.69, \quad c_1 = 1826.15$$

$$a_2 = -93.375, \quad b_2 = -484.32, \quad c_2 = 1275.2.$$

Rearrangement of equations (7), (13) and (14), followed by substitution into (8), yields a cubic polynomial in melt fraction, dependent on enthalpy and bulk composition, which can be solved analytically

$$\phi = \frac{h}{L_f} - \frac{c_P}{L_f}\left(\frac{c_k + \left(\left(2a_k\left(\frac{C - C_S + C_S\phi}{\phi}\right) + b_k\right)^2 + b_k^2\right)}{4a_k}\right) \tag{15}$$

where a_k, b_k and c_k are the constants given above. The solid solution compositions are described by

$$C_L = \frac{-b_3 + \sqrt{b_3^2 - 4a_3(c_3 - T)}}{2a_3} \tag{16}$$

$$C_S = \frac{-b_4 + \sqrt{b_4^2 - 4a_4(c_4 - T)}}{2a_4} \tag{17}$$

$$a_3 = -466, \quad b_3 = -135.69, \quad c_3 = 1826.15$$

$$a_4 = -93.375, \quad b_4 = -484.32, \quad c_4 = 1275.25.$$

Rearrangement of equations (7), (16) and (17), and substitution into (8), yields an expression for the melt fraction in terms of enthalpy and bulk composition. This is solved numerically using the Newton-Raphson method.

Initial and Boundary Conditions

Three cases have been modeled with different initial and boundary conditions (fig. 1). In the first case, the temperature in the column is instantaneously brought to a value above the solidus, $T_i > T_S$, at $t = 0$, yielding a constant initial melt fraction, $\phi_i > 0$. The solidus temperature corresponds to the eutectic in the eutectic phase diagram (fig. 2A) and the solidus temperature of component B in the solid-solution phase diagram (fig. 2B). The initial composition is homogenous (fig. 1A) or contains two layers of different initial composition (fig. 1B). Heat is not allowed to enter or leave the column, so

$$\frac{\partial T}{\partial z} = 0, \quad z = 0, z_{Mi} \tag{18}$$

where z_{Mi} is the top of column. At the base of the column, there is no flow of melt or matrix, so

$$w_S = w_L = 0, \quad z = 0. \tag{19}$$

The uppermost surface of the mush moves downwards with time and, on this surface, there is no compaction, so

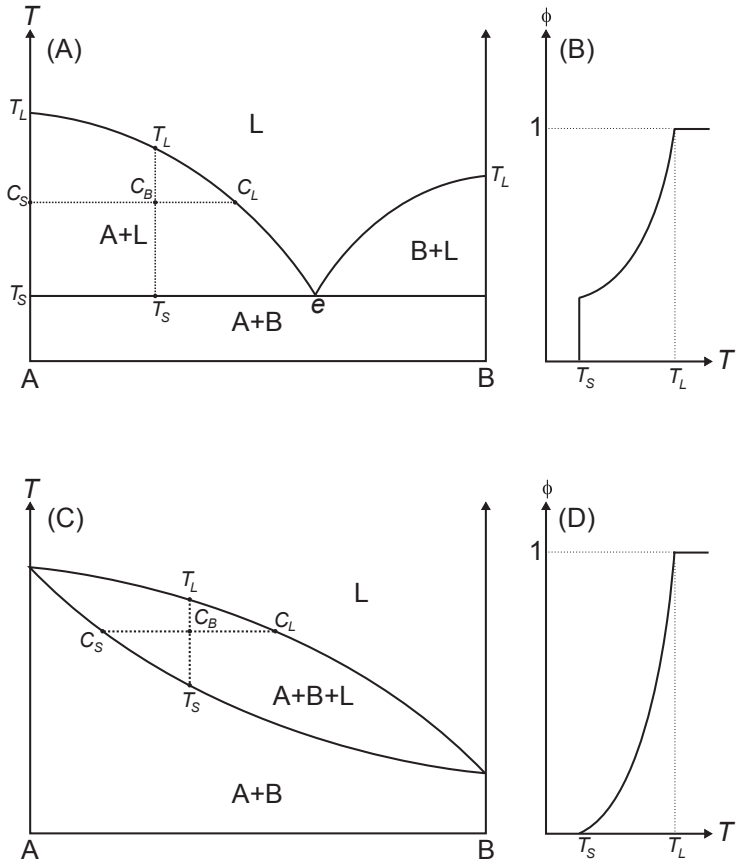

Fig. 2. (A) Example binary eutectic phase diagram. A and B refer to the separate components, L the liquid and *e* is the eutectic point; bulk composition C_B yields the relationship between melt fraction and temperature shown in (B). (C) Example solid solution phase diagram; bulk composition C_B yields the relationship between melt fraction and temperature shown in (D). Modified from Hillert (2007).

$$\frac{\partial w_S}{\partial z} = 0, \quad z = z_M \tag{20}$$

where z_M is the top of the mush at time t.

In the second case, the column is initially at a temperature below the solidus, $T_i < T_S$, yielding $\phi_i = 0$. Heat is allowed to enter through the base of the column, which may be initially homogenous (fig. 1C) or contain two layers of different initial composition (fig. 1D). At $t = 0$, the temperature at the base is increased to the mid-value between the solidus and liquidus temperatures, and subsequently stays fixed for all time, yielding the boundary conditions

$$\begin{aligned} \frac{\partial T}{\partial z} &= 0, \quad z = z_{Mi} \\ T &= \frac{T_L - T_S}{2} + T_S, \quad z = 0. \end{aligned} \tag{21}$$

The liquidus temperature corresponds to the liquidus of component A in both phase diagrams (fig. 2). The boundary conditions on velocity are given by

$$w_S = w_L = 0, \quad z = 0, z_{Mi}. \tag{22}$$

In the third case (fig. 1E), the temperature in the column is initially above the solidus, $T_i > T_S$, at $t = 0$, yielding a constant initial melt fraction, $\phi_i > 0$. Heat is allowed to leave each end of the column, corresponding to cooling from above and below. At $t = 0$, the temperature at the base and top of the column is decreased and subsequently stays fixed for all time, with the boundary conditions

$$T = 2T_S - T_i, \quad z = 0, z_{Mi}. \tag{23}$$

The boundary conditions on velocity are given by equation (22).

Solution of the Governing Equations

The governing equations are non-dimensionalized using characteristic time- and length-scales modified from McKenzie (1984) and Jackson and others (2003)

$$k'_\phi = k_\phi / K_\phi = \phi^\alpha, \quad K_\phi = a^2 b \tag{24}$$

$$w' = w/\omega, \quad \omega = \frac{K_\phi \Delta\rho g}{\mu} \tag{25}$$

$$z' = z/\delta, \quad \delta = \left(\frac{\eta_0 K_\phi}{\mu}\right)^{\frac{1}{2}} \tag{26}$$

$$t' = t/\tau, \quad \tau = \frac{1}{\Delta\rho g}\left(\frac{\mu\eta_0}{K_\phi}\right)^{\frac{1}{2}} \tag{27}$$

$$T' = \frac{T - T_S}{T_L - T_S} \tag{28}$$

$$h' = \frac{h - h_S}{h_L - h_S} \tag{29}$$

where the solidus and liquidus temperature for each phase diagram are defined above, and the same definitions apply to the enthalpy. Substitution of equations (24)–(29) into (1)–(6) and dropping of primes yields the final dimensionless equations

$$\frac{\partial h}{\partial T} = \kappa_{eff}\frac{\partial^2 T}{\partial z^2} + Ste\frac{\partial}{\partial z}((1-\phi)w_S) \tag{30}$$

$$\frac{\partial C}{\partial t} = \frac{\partial}{\partial z}((1-\phi)w_S C_S) - \frac{\partial}{\partial z}(\phi w_L C_L) \tag{31}$$

$$\frac{\partial I}{\partial t} = \frac{\partial}{\partial z}((1-\phi)w_S I_S) - \frac{\partial}{\partial z}(\phi w_L I_L) \tag{32}$$

$$\frac{\partial}{\partial z}\left(\phi^{-\beta}\frac{\partial w_S}{\partial z}\right) = \frac{w_S}{\phi^\alpha} + (1-\phi). \tag{33}$$

The dimensionless scaling factor κ_{eff} in (eq 30) is given by

$$\kappa_{eff} = \frac{k_T \tau (T_L - T_S)}{\rho \delta^2 (c_P (T_L - T_S) + L_f)} \tag{34}$$

and the Stefan number by

$$Ste = \frac{L_f}{(c_P (T_L - T_S) + L_f}. \tag{35}$$

Solid and liquid velocities are related to each other through

$$\phi w_L = -(1 - \phi) w_S. \tag{36}$$

The boundary conditions (eq 21) and (eq 23) become

$$\begin{aligned} \frac{\partial T}{\partial z} &= 0, \quad z = z_{Mi} \\ T &= 0.5, \quad z = 0 \end{aligned} \tag{37}$$

$$T = -0.3, \quad z = 0, z_{Mi}. \tag{38}$$

Equations (30)–(33) are solved numerically using finite difference methods and a code developed by the authors. Equation (30) is approximated using a forward-time centered-space scheme, equations (31) and (32) using a second-order Lax-Wendroff scheme and equation (33) using a centered scheme (Morton and Meyers, 2005). Energy conservation (eq 30) and component conservation (eqs 31, 32) are solved first. The porosity (equivalent to melt fraction) and temperature are then updated as determined by local thermodynamic equilibrium. Finally, velocity is solved (eq 30) and the system is updated for the next time step.

Material Properties

The material properties required are the phase diagrams (fig. 2), and the values of just four dimensionless parameters that entirely characterize the system: κ_{eff}, *Ste*, and the exponents governing permeability and viscosity. Physically, κ_{eff} characterizes the relative transport rates of heat and mass (via compaction). When κ_{eff} is very large ($\gg$10), heat transport is rapid relative to mass transport, so melt fractions tend towards those that would be observed if there were no melt migration, and compositions tend towards those obtained by batch melting; when κ_{eff} is very small ($\ll 10^{-4}$), mass transport is rapid compared to heat transport (Jackson and Cheadle, 1998). However, for a broad range of intermediate values of κ_{eff}, appropriate for crustal igneous systems $10^{-4} < \kappa_{eff} < 10$), both heat and mass transport are important and their relative rates dictate the temporal and spatial evolution of temperature and melt fraction (Jackson and others, 2003, 2005). The value of κ_{eff} we use here is typical of crystal mushes in the crust (see table 2 and Jackson and others, 2003, 2005); as we show later in the paper, similar results are obtained if κ_{eff} is varied over the range likely to be observed in these systems, depending primarily upon melt viscosity, mush grain size, and mush bulk and shear viscosities (eqs 34 and 24, 26, 27). *Ste* varies over the range $0 \leq Ste \leq 1$, and the chosen value has a minor impact on melting and melt migration (Jackson and Cheadle, 1998). Our most significant assumption is that the material properties (and, hence, the value of κ_{eff}) remain constant regardless of temperature and composition. In many crustal systems, and for several of the material properties, this is unlikely to be the case; for example, melt viscosity, mush shear and bulk viscosities, and thermal conductivity, will all likely vary with temperature and composition (for example Whittington and others, 2009; Nabelek and others, 2012) although the effect of compositional variations on viscosity may be buffered by the presence of volatiles such

TABLE 2

Material properties used to produce the dimensionless results

Symbol	Description	Value
α	permeability exponent	3
β	viscosity exponent	0.5
k_{eff}	effective thermal diffusivity	3.84×10^{-2} ($3.84 \times 10^{-4} - 3.84$)
Ste	Stefan number	0.237

The range of values of k_{eff} shown in brackets is investigated later in the paper, and is representative of crustal igneous mushes (Jackson and others, 2003, 2005).

as water (see, for example, Clemens and Petford, 1999). However, assuming constant material properties allows the impact of phase change and chemical reaction on melt fraction and composition to be clearly demonstrated, using simple, dimensionless results, and does not affect the conclusions we draw from these.

RESULTS

All results are presented in dimensionless form. A temperature of $T = 0$ corresponds to the solidus; a temperature of $T = 1$ corresponds to the liquidus. Likewise, a composition of $C = 0$ corresponds to component A; a value of $C = 1$ corresponds to component B. A composition of $C = 0.2$ therefore contains 80 percent A and 20 percent B.

Constant Initial Temperature with No Cooling in an Initially Homogenous Column

We begin by simulating compaction in a perfectly insulated column with uniform initial temperature $T_i = 0.1$ and melt fraction $\phi_i = 0.2$ (fig. 1A). A solution to this problem, in the absence of component transport, was presented by Richter and McKenzie (1985) and we use this to validate our numerical solutions, obtaining a good match (fig. 3). We then investigate how the results are affected by component transport and chemical reaction. In the eutectic case, the initial bulk composition is $C_i = 0.12$, which yields an initial composition of $C_{Li} = 0.605$ and an initial solid composition of $C_{Si} = 0$ (that is, pure A) (fig. 4). In the solid-solution case, an initial bulk composition of $C_i = 0.51$ is required to obtain the same T_i and ϕ_i. This bulk composition yields an initial melt composition of $C_{Li} = 0.755$ and initial solid composition of $C_{Si} = 0.448$ (fig. 5). The initial concentration of trace elements in the solid phase is $I_i = 1$.

In all cases, regardless of whether component transport is included, and regardless of which phase diagram is used to model component transport, we find that the melt fraction decreases at the base of the column as buoyant melt migrates upwards and the solid compacts in response, and a pure melt layer forms at the top of the column. The top of the mush moves downwards (seen in figs. 3, 4B and 5B). Moreover, the local bulk composition (that is, the local composition of melt + solid) at the top of the column becomes enriched in component B, as the melt (which is enriched in B) migrates upwards and accumulates in the melt layer. However, when component transport is omitted, the temperature and melt composition in the (perfectly insulated) column remain constant (dotted lines in figs. 4A, 4D; 5A, 5D); there is no further chemical reaction after the initial melt distribution is established, so the melt composition remains at its initial value, which corresponds to batch melting (dotted lines in figs. 4D and 5C and 5D). In contrast, when component transfer is included, temperature and melt composition vary through the column; the temperature decreases relative to the initial value (figs. 4A and 5A) and the melt composition becomes

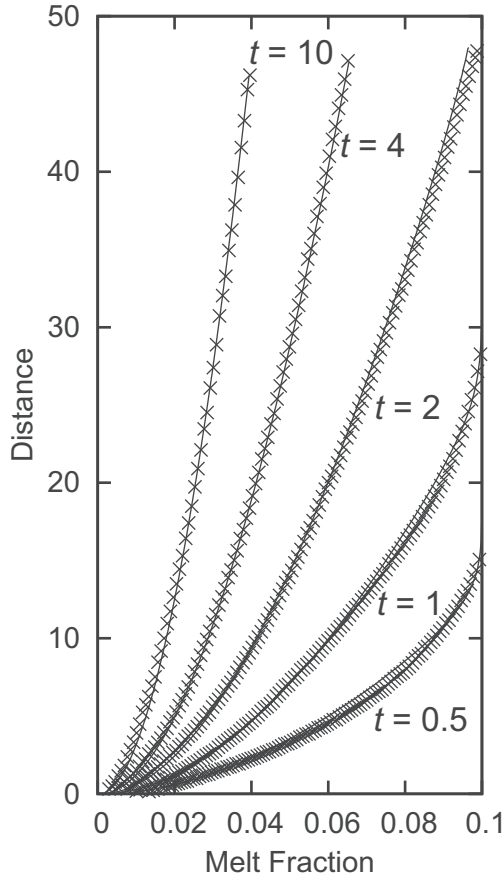

Fig. 3. Comparison of our model results (crosses) with those of Richter and McKenzie (1985) (solid lines) for a column with constant initial melt fraction and no component transport, at various dimensionless times.

more enriched in B compared to the batch melting case (figs. 4D and 5D); the most significant deviations are observed at the base of the column, and propagate upwards through time. Regardless of the phase diagram used, melt migration causes changes in local bulk composition which, when component transport is accounted for, lead to changes in temperature and melt composition. Local enrichment in the refractory A component at the base of the column, where melt leaves the system, results in melting to remain in local equilibrium; this causes variations in melt composition and temperature. At each point in the column, there is a fixed amount of heat that was added (instantaneously) at $t = 0$, which is partitioned between latent and sensible heat. Phase change occurs only through conversion of latent to sensible heat and vice-versa. Melting converts sensible heat to latent heat, causing the cooling observed at the base of the column.

Figure 6 shows the concentrations of incompatible (upper plots A-F) and compatible (lower plots G-L) elements at a single snapshot in time ($t = 120$), using the eutectic phase diagram to model major component transport (that is, corresponding to fig. 4). When component transport is omitted, the trace element concentration remains constant, because there is no further chemical reaction after the initial melting event

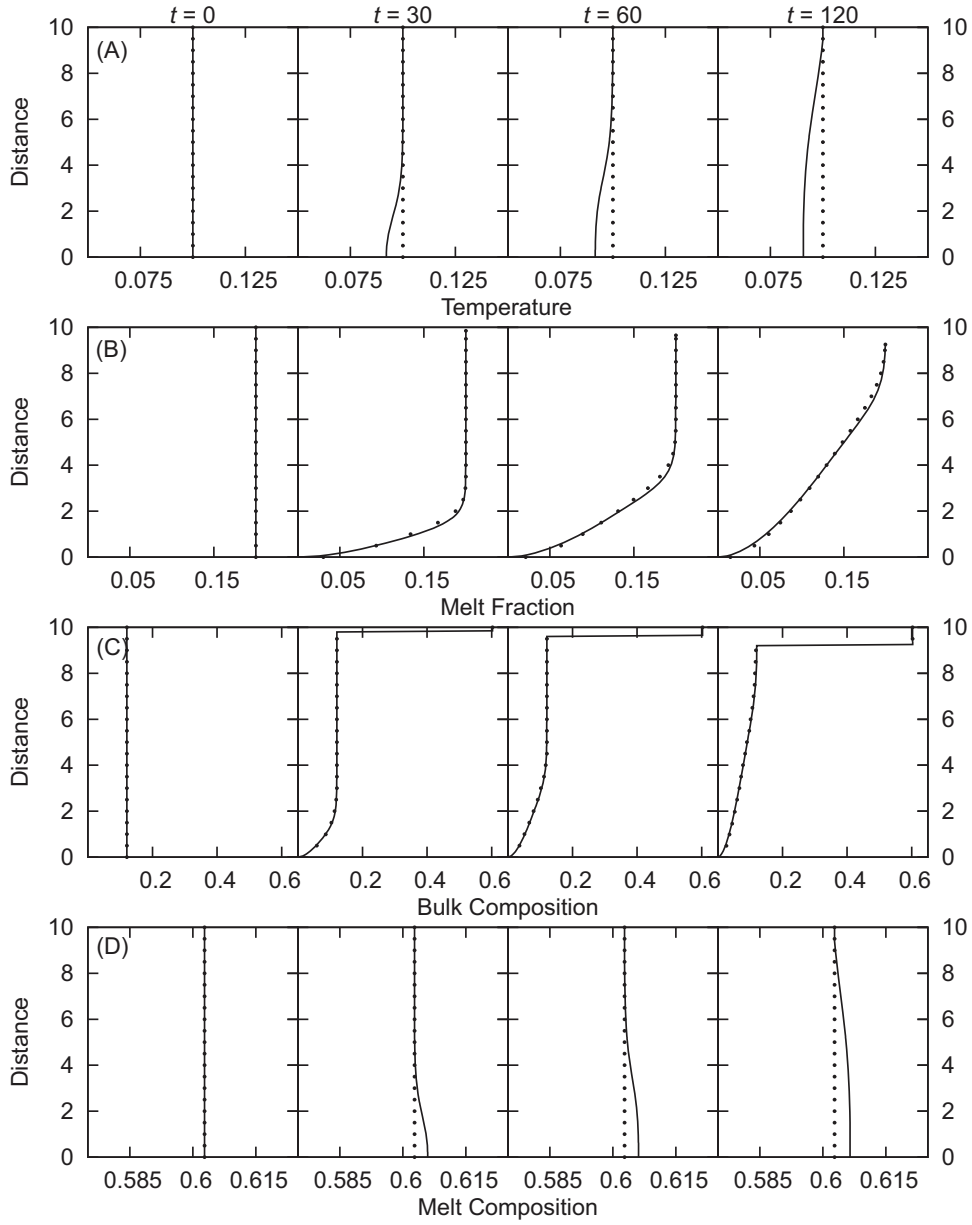

Fig. 4. (A) Temperature, (B) melt fraction, (C) bulk composition and (D) melt composition at $t = 0$, 30, 60 and 120, for an initially homogeneous column with $T_i = 0.1$, $\phi_i = 0.2$ and $C_i = 0.12$, governed by the eutectic phase diagram (fig. 2A). The eutectic composition is $e = 0.6417$. Solid lines show the results when component transport is included; dots show the results when component transport is neglected. The solid composition is not shown and is constant with a value of 0 (pure component A). Note that bulk composition in this and all subsequent figures denotes the local composition, which varies from the initial composition because of melt migration.

(squares); the concentration is fixed throughout the column at its initial value, which corresponds to batch melting. However, when component transport is included, bulk concentration varies through the column. For incompatible trace elements, both melt

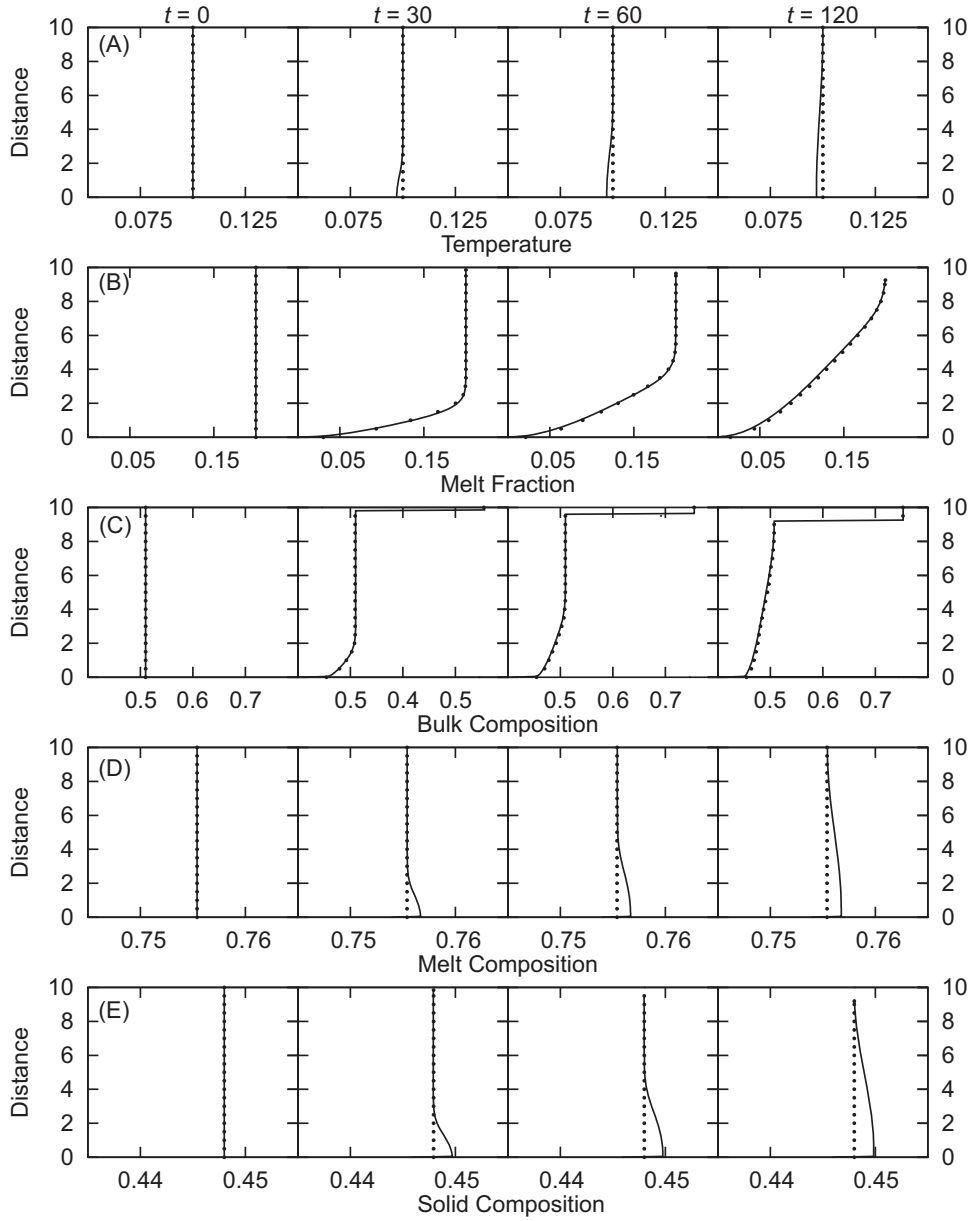

Fig. 5. (A) Temperature, (B) melt fraction, (C) bulk composition, (D) melt composition and (E) solid composition at $t = 0$, 30, 60 and 120, for an initially homogeneous column with $T_i = 0.1$, $\phi_i = 0.2$ and $C_i = 0.49$, governed by the solid solution phase diagram (fig. 2B). Solid lines show the results when component transport is included; dots show the results when component transport is neglected.

concentration and solid concentration decrease at the base of the column (figs. 6A-6F); the opposite is true for compatible trace elements, although the change is smaller in magnitude (figs. 6G-6L). Differences in trace element concentration from the batch melting case become relatively more significant as the partition coefficient decreases for incompatible elements, and increases for compatible elements. As the

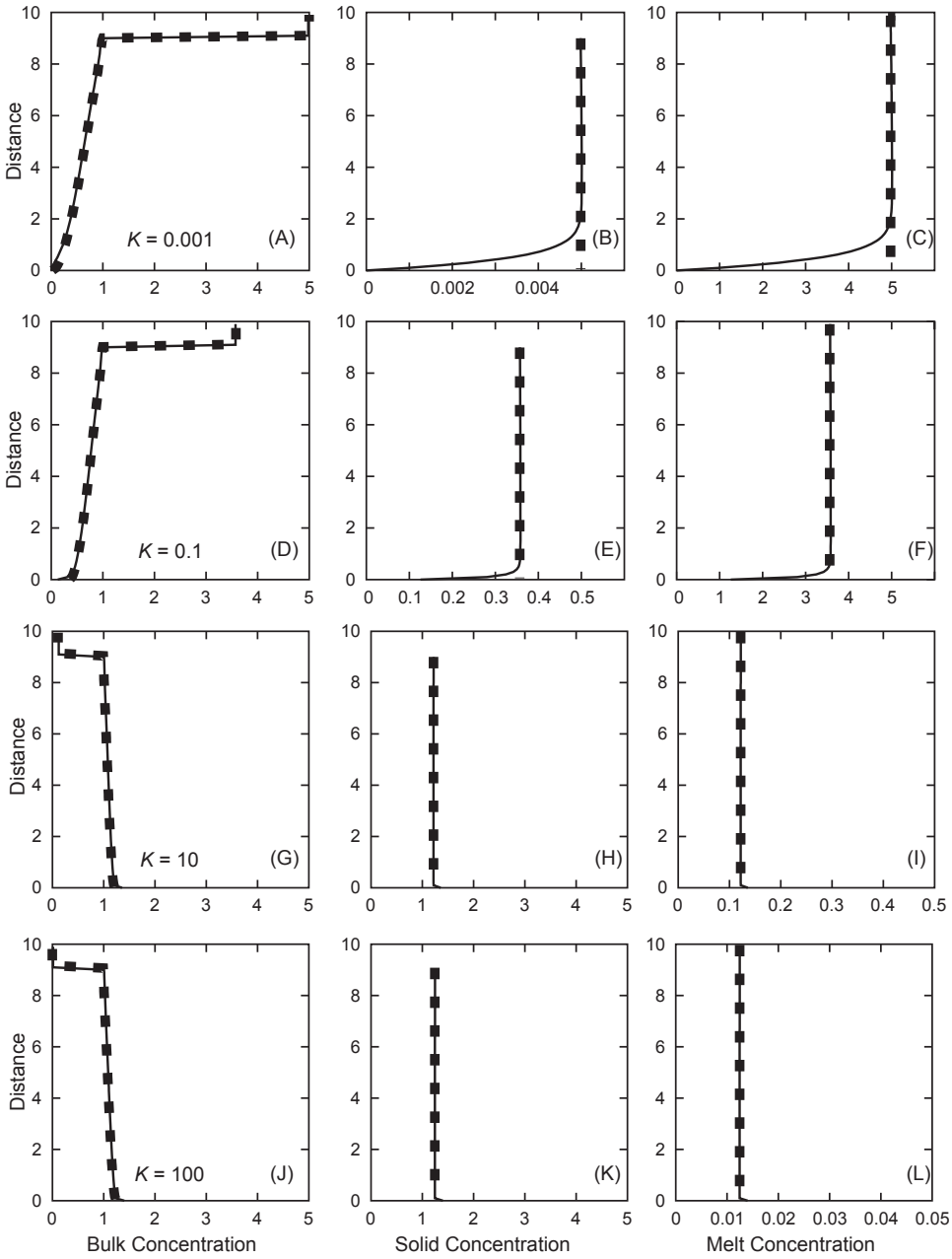

Fig. 6. Bulk, solid, and melt trace element concentrations for an initially homogeneous column with uniform trace element distribution $I_i = 1$ at $t = 120$, for both incompatible ($K = 0.001$ and $K = 0.1$) and compatible ($K = 10$ and $K = 100$) trace elements. Melting is governed by the eutectic phase diagram; the results shown here correspond to those at $t = 120$ in figure 4. Solid lines show the results when component transport is included; squares show the results when component transport is neglected.

bulk concentration of incompatible elements decreases, the overlying column becomes enriched, leading to variations in the trace element concentration of the melt expelled from the mush (fig. 7; the expelled melt corresponds to the melt that

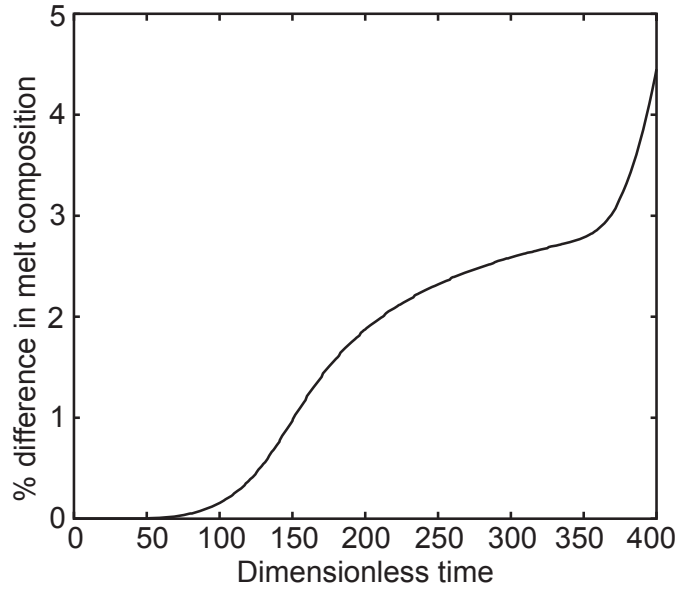

Fig. 7. Percentage enrichment in incompatible (K = 0.001) trace element concentration in melt expelled from the top of the compacting column shown in figures 4 and 6, relative to a model of compaction that omits chemical reaction.

accumulates in the pure melt layer at the top of the column). In this case, component transport produces melt that is more enriched in incompatible elements than predicted by batch melting.

These results show that simple batch melting fails to describe major and trace element compositions. Component transport leads to spatial variations in major element composition (represented by components A and B) as melt migrates through, and reacts with, the crystalline mush; moreover, component transport changes the trace element composition of the melt that leaves the mush. In the results we show here, differences in major and trace element composition from those predicted by batch melting are small (<5%). However, they become much larger in more complex models in which melts migrate through a heterogeneous column. These are considered in the next section.

Constant Initial Temperature with No Cooling in an Initially Heterogeneous, Two-Layer Column

We now consider a column comprising two layers with initial solid composition of pure A in the lower half and pure B in the upper half (fig. 1B), described by the eutectic phase diagram. At $t = 0$, $C_i = 0.12$ in the lower half of the column ($0 \leq z < 5$) and $C_i = 0.95$ in the upper half of the column ($5 \leq z \leq 10$) (fig. 8). These initial bulk compositions have been chosen so that at the (uniform) initial temperature ($T_i = 0.1$) there is a constant melt fraction in the column ($\phi_i = 0.2$). Any variation in melt fraction is therefore due to melt migration and component transport. As found in the homogenous model (fig. 4B), melt fraction decreases at the base of the column, regardless of whether component transport is included (solid lines) or omitted (dashed lines) as the buoyant melt migrates upwards to accumulate in a melt layer at the top of the column and the matrix compacts in response (fig. 8B); moreover, the bulk composition becomes enriched in A at the base of the column (fig. 8C). However,

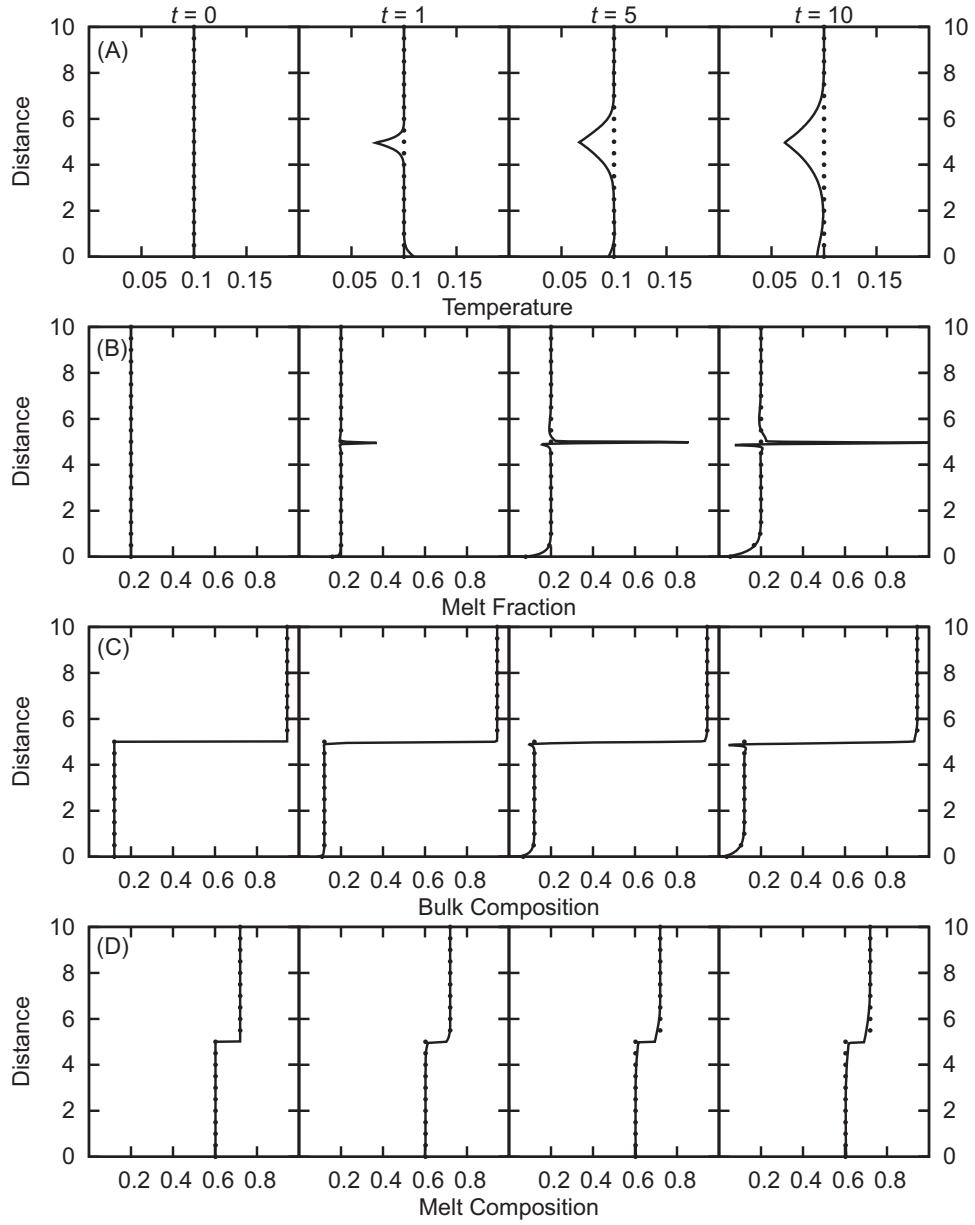

Fig. 8. (A) Temperature, (B) melt fraction, (C) bulk composition and (D) melt composition at $t = 0$, 30, 60 and 120, for an initially heterogeneous column with $T_i = 0.1$ and $\phi_i = 0.2$, governed by the eutectic phase diagram (fig. 2A). The initial bulk composition is $C_i = 0.12$ for $0 \leq z < 5$ and $C_i = 0.95$ for $5 \leq z \leq 10$; the eutectic composition is $e = 0.6417$. Solid lines show the results when component transport is included; dots show the results when component transport is neglected. The solid composition is not shown and is constant with a value of 0 (pure component A).

when component transport is included, a high melt fraction forms at the interface between the two layers of different initial composition and, by $t = 5$, the melt fraction here exceeds 0.8. The high melt fraction layer moves downwards with time, and

increases in amplitude and thickness. The temperature at the location of the high melt fraction also decreases (fig. 8A). Without component transport, no melt layer forms at the interface, and the temperature remains constant.

Melt migration and component transport leads here to the development of a compositionally mixed region at the interface between the two layers that increases in thickness with time. As melt migrates upwards and the mush compacts in response, crystals of B migrate downwards and mix with melt migrating upwards that was initially in equilibrium with crystals of A. Melting of B occurs to restore equilibrium, producing a high melt fraction; the associated cooling is caused by the conversion of sensible to latent heat. This leads to a highly counter-intuitive result, in which melt fraction increases as temperature decreases, as a consequence of reactive transport changing the local bulk composition. The resulting temperature is close to the solidus, but a large melt fraction is present because the local bulk composition is close to the eutectic ($e = 0.64$). This mechanism for producing high melt fractions in layered systems has not been predicted before, and is not captured by models that omit component transport.

Heating from Below of an Initially Solid and Homogenous Column

We now consider a homogeneous column which is heated from below, to mimic melt generation in deep crustal hot zones and in the cumulate pile within some layered intrusions (fig. 1C). The column is initially at a temperature below the solidus, $T_i = -0.1$; at $t = 0$, the temperature at the base of the column is fixed at a value of $T_{z=0} = 0.5$ and does not vary with time. Heat therefore enters the column through the base, but does not leave the column because the other three sides are perfectly insulated. As before, the initial bulk composition in the eutectic case is $C_i = 0.12$ (fig. 9); however, the initial bulk composition in the solid-solution case is $C_i = 0.45$, to yield consistent values of T_S and $T_{z=0}$ (fig. 10). The initial composition of trace elements is $I_i = 1$. Regardless of the phase diagram used, we find that a partially molten zone forms at the base of the column that grows in thickness through time as the solidus isotherm migrates upwards (figs. 9A and 10A). High melt fraction layers are formed that rise through the column (figs. 9B and 10B). Similar behavior has been observed in models that omit component transport (Jackson and Cheadle, 1998; Jackson and others, 2003, 2005; Solano and others, 2012). The melt layers form when the melt flux decreases upwards in response to the upwards decrease in melt fraction and permeability towards the solidus isotherm, which acts as a barrier to melt flow at the top of the partially molten zone. Melt locally accumulates when the melt flux decreases upwards, and the matrix dilates to accommodate it, resulting in the formation of a melt layer (Jackson and Cheadle, 1998).

Regardless of the phase diagram used, the local bulk composition evolves in response to melt migration, becoming enriched in B ($C = 1$) in the melt layer where there is a net accumulation of melt, but depleted in B at the base of the column where there is a net loss of melt (figs. 9C and 10C). Melt composition is determined by the temperature, so is also enriched in B at the top of the partially molten layer where the temperature is lower (figs. 9D and 10D). As melt rises, it cools and changes composition. For the eutectic phase diagram, the temperature at the location of the high melt fraction layer is close to the solidus, so the melt layer contains melt of close to eutectic ($e = 0.64$) composition. This melt has the same composition as that produced during batch melting to the same temperature, but has accumulated to form a much higher melt fraction layer (of melt fraction $\phi = 0.6$). Batch melting (that is, without melt migration and component transport) can produce eutectic melt to a maximum fraction of only $\phi = 0.1875$ for the chosen initial bulk composition. Thus, melt segregation during heating from below provides a mechanism to accumulate and mobilize evolved melt, with a composition corresponding to a (much) smaller degree

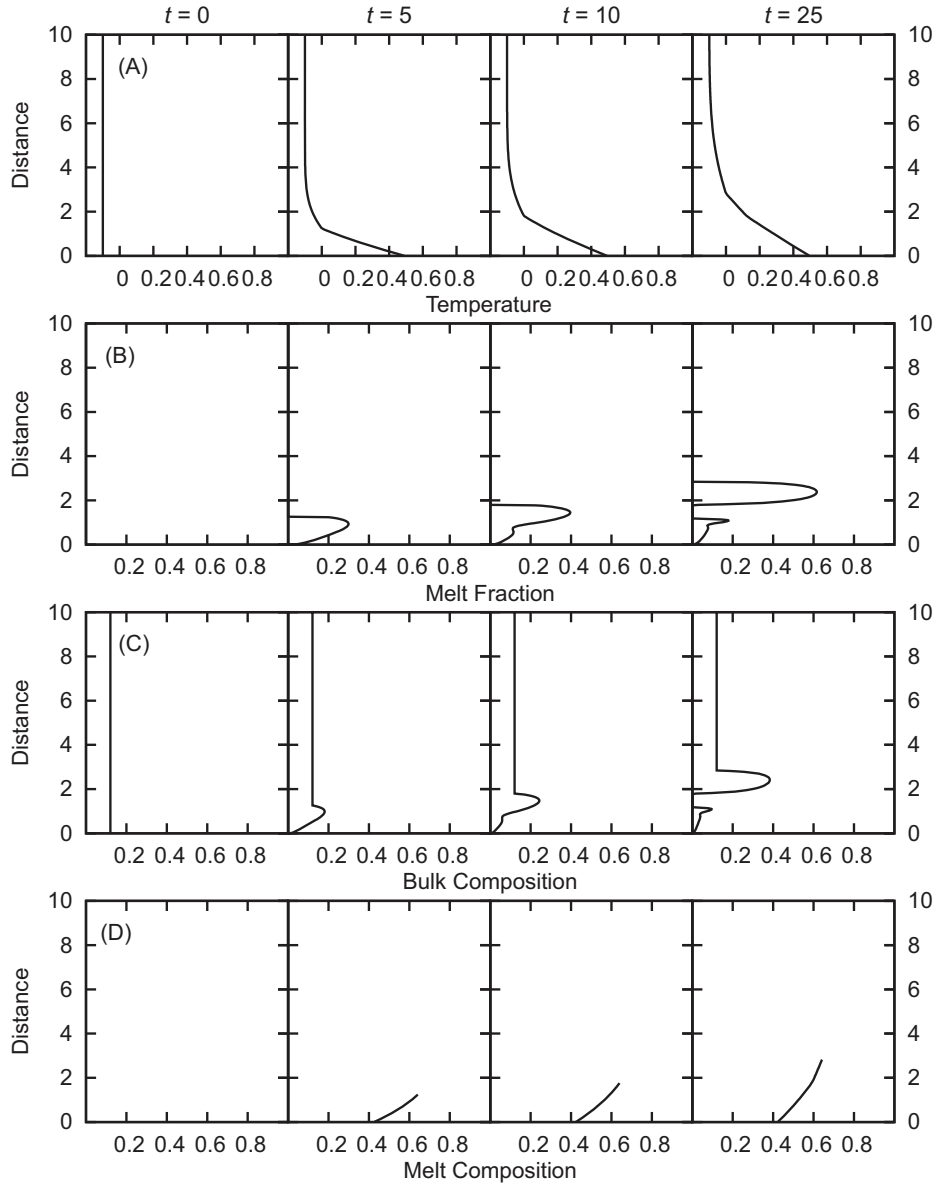

Fig. 9. (A) Temperature, (B) melt fraction, (C) bulk composition and (D) melt composition at $t = 0$, 5, 10 and 25, for an initially homogeneous column with $T_i = -0.1$, $\phi_i = 0$ and $C_i = 0.12$, governed by the eutectic phase diagram (fig. 2A). The column is heated from below with $T_{z=0} = 0.5$ for all time. The solid composition is not shown, and is constant at $C = 0$ (pure component A) in the partially molten zone (where $T > T_S$), or at the initial composition $C = C_i$ in the solid zone (where $T \leq T_S$). Where the melt fraction is zero the melt composition is not defined, hence the discontinuous lines in (D).

of batch (static) melting. The solid composition (not shown) is pure A at all temperatures above the solidus, a mixture of A and B at the solidus, and the initial bulk composition at temperatures below the solidus. At the base of the column, the mush becomes refractory and unable to produce further melt, because of depletion in B. As

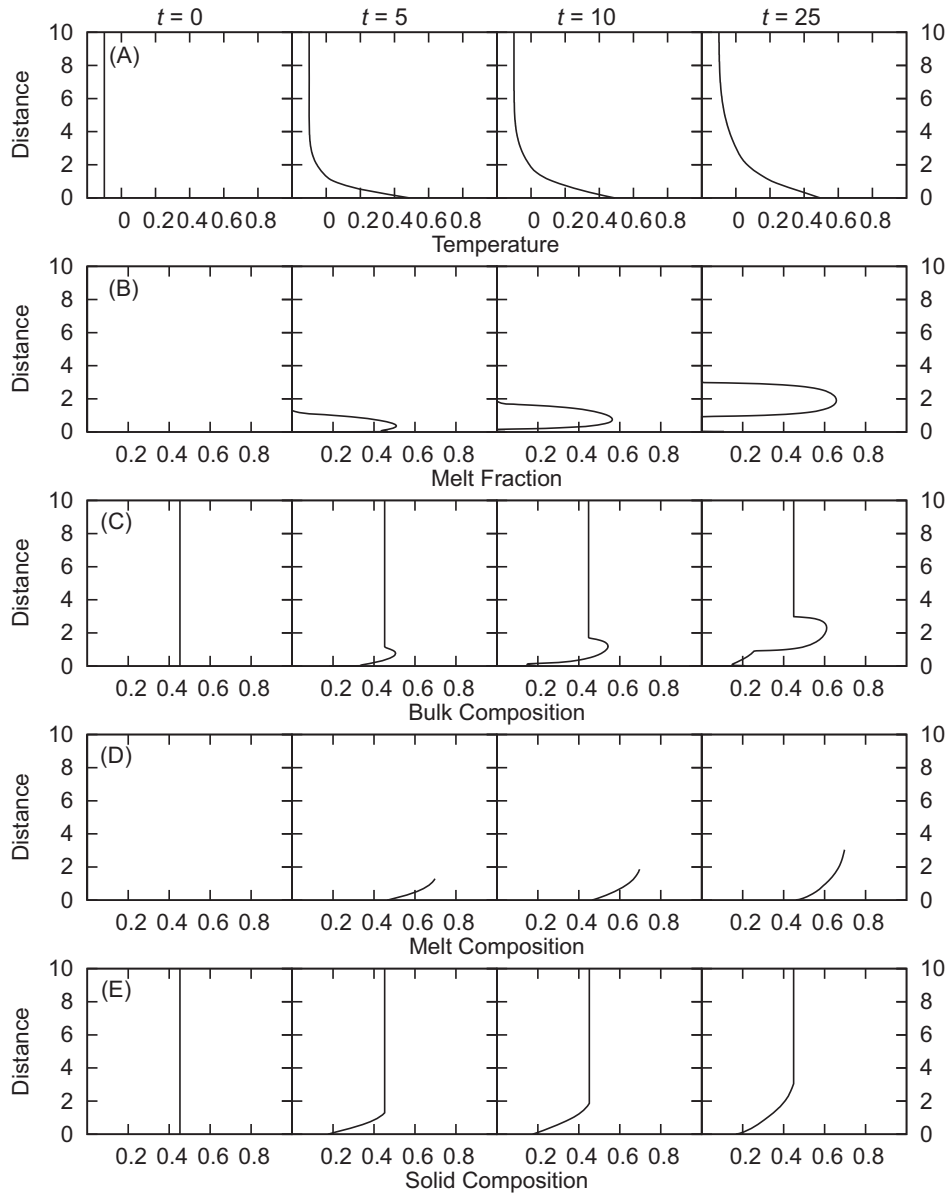

Fig. 10. (A) Temperature, (B) melt fraction, (C) bulk composition, (D) melt composition and (E) solid composition at $t = 0$, 5, 10 and 25, for an initially homogeneous column with $T_i = -0.1$, $\phi_i = 0$ and $C_i = 0.49$, governed by the solid solution phase diagram (fig. 2B). The column is heated from below with $T_{z=0} = 0.5$ for all time.

melt migration drives the bulk composition towards A, the temperature required to produce melt increases. Eventually, the temperature at the base of the column is too low for any further melt to be produced.

For the solid solution phase diagram, both solid and melt compositions become enriched in B towards the top of the partially molten zone (figs. 10D and 10E). The

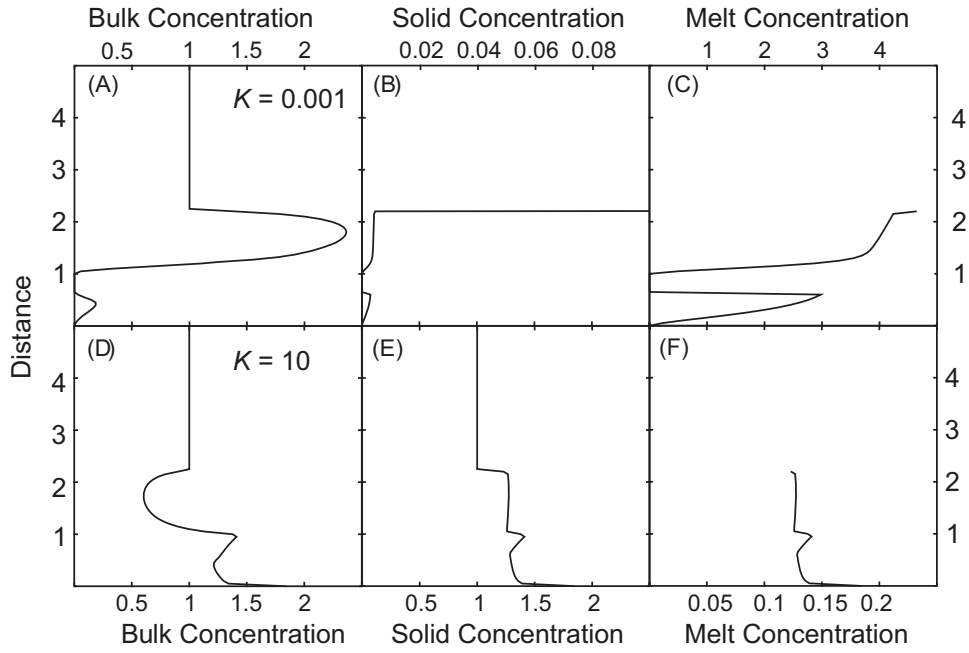

Fig. 11. Bulk, solid, and melt trace element concentrations for an initially homogeneous column with uniform trace element distribution $I_i = 1$ at $t = 0$, for both incompatible ($K = 0.001$) and compatible ($K = 10$) trace elements. The column is heated from below with $T_{z=0} = 0.5$ for all time. Melting is governed by the eutectic phase diagram; the results shown here correspond to those at $t = 25$ in figure 9.

high melt fraction layer contains melt with a composition of $C = 0.8$ and a melt fraction of $\phi = 0.6$. Batch melting can produce melt of this composition to a maximum fraction of $\phi = 0.215$ for the chosen initial bulk composition; melt segregation leads to accumulation of this melt to a much higher melt fraction. As in the eutectic case, melt segregation during heating from below provides a mechanism to accumulate and mobilize melt with a composition corresponding to a (much) smaller degree of batch melting. Solid composition is temperature-dependent for the solid-solution phase diagram, so the solid becomes enriched in A as the temperature increases, unlike the eutectic case. The generation of a refractory layer at the base of the column, with composition $C = 0.2$, is observed for the solid solution, similar to the eutectic case. However, further increasing the temperature at the base above $T = 0.5$ still produces melt for the solid-solution phase diagram, whereas in the eutectic case, a large increase in temperature to $T = 1$ is required to generate additional melt, as the residue is pure A.

Figure 11 shows the concentration of trace elements in the bulk, solid and melt, at a single snapshot in time ($t = 25$), using the eutectic phase diagram to model major component transport (that is, corresponding to fig. 9). As melt migrates upwards through the column and accumulates in the high porosity melt layer, incompatible trace elements transported in the melt become enriched in the melt layer relative to the initial bulk concentration, yielding the upper peak in concentration (fig. 11C). However, some melt remains at the base of the column, at very low melt fraction, which cannot be "squeezed out" of the mush during compaction; thus melt enriched in incompatible trace elements becomes trapped in the refractory solids at the base, yielding the lower peak in melt concentration (fig. 11C). The local bulk and solid compositions at the base of the column become depleted in trace elements, as

incompatible elements enter the melt and migrate upwards (figs. 11A and 11B). However, the presence of the trapped, incompatible element-rich melt fraction towards the base of the column means that the bulk composition in this region is enriched in incompatibles compared to the predictions of batch and fractional melting models (see the lower peak in fig. 11A). Compatible trace elements entering the solid are transported downwards during compaction, so the base of the column becomes enriched in these relative to the initial bulk concentration (figs. 11D and 11E).

Melt migration and component transport significantly affects the trace element concentration of the melt that accumulates in the melt layer (fig. 12). Here, we plot the peak melt fraction, and the trace element composition of the melt at the location of the peak melt fraction, and compare these with the equivalent values for melt with the same major element composition (that is, same value of C), predicted using batch and fractional melting models. Incompatible trace elements are *less* enriched in melt that accumulates in a melt layer during melt migration, compared to melt of the same major element composition produced through batch or fractional melting; indeed, incompatible concentrations can be half that predicted by batch and fractional melting models. Note the contrast with the earlier result for a column of uniform initial temperature, in which melt expelled from the top of the column was *more* enriched in incompatible elements relative to batch and fractional melting models (fig. 7). Reactive flow leads to deviations in melt chemistry from these model predictions, but the deviations depend upon the temperature gradient through which the melt is migrating. Here, melt segregation during heating from below provides not only a mechanism to accumulate evolved melt (with a major element composition corresponding to a (much) smaller degree of batch (static) melting) in high porosity layers, but also to decouple the fractionation of major and trace elements. The melt that accumulates in the high porosity layers is less enriched in incompatible elements than would be expected for the same major element concentration, assuming batch or fractional melting.

Heating from Below of an Initially Solid and Heterogeneous Two-Layer Column

We now consider a column with two layers heated from below for the eutectic case, with initial solid composition of pure A in the lower half ($0 \leq z < 5$) and pure B in the upper half ($5 \leq z \leq 10$) (fig. 1D). As before, the column is initially at a temperature below the solidus, $T_i = -0.1$; at $t = 0$, the temperature at the base of the column is fixed at a value of $T_{z=0} = 0.5$ and does not vary with time. This system is dominated by the evolution and interaction of high porosity melt layers created by two different mechanisms (fig. 13). The first is the melt layer resulting from melt migration upwards though a temperature gradient, as observed in the homogenous column heated from below (fig. 9); the second is the melt layer created by mixing at the interface between the two different initial compositions, as observed in the uniformly heated column (fig. 8). Once the upwards migrating melt layer reaches the compositional interface, a large volume of melt is rapidly generated and the melt fraction increases to $\phi = 1$ (that is, a pure melt layer is formed; fig. 13B). The melt in this layer has a bulk composition close to the eutectic ($e = 0.64$) (fig. 13C). Generation of this melt at the interface requires the conversion of sensible to latent heat, which causes the solidus isotherm to be "pinned" at the interface until melting is complete (fig. 13A). Only when all of component B in the solid phase has been exhausted does the temperature in the upper half of the column begin to increase, at which time melt migrates into, and begins to accumulate within, the upper layer. Thus compositional heterogeneity can impact on the rate at which heat diffuses during melting; it can also yield high fractions of evolved melt (that is, with a major element composition corresponding to a small degree of batch melting). Although not shown here, melt that accumulates in the high melt fraction layers is less enriched in incompatible elements than would be expected if the

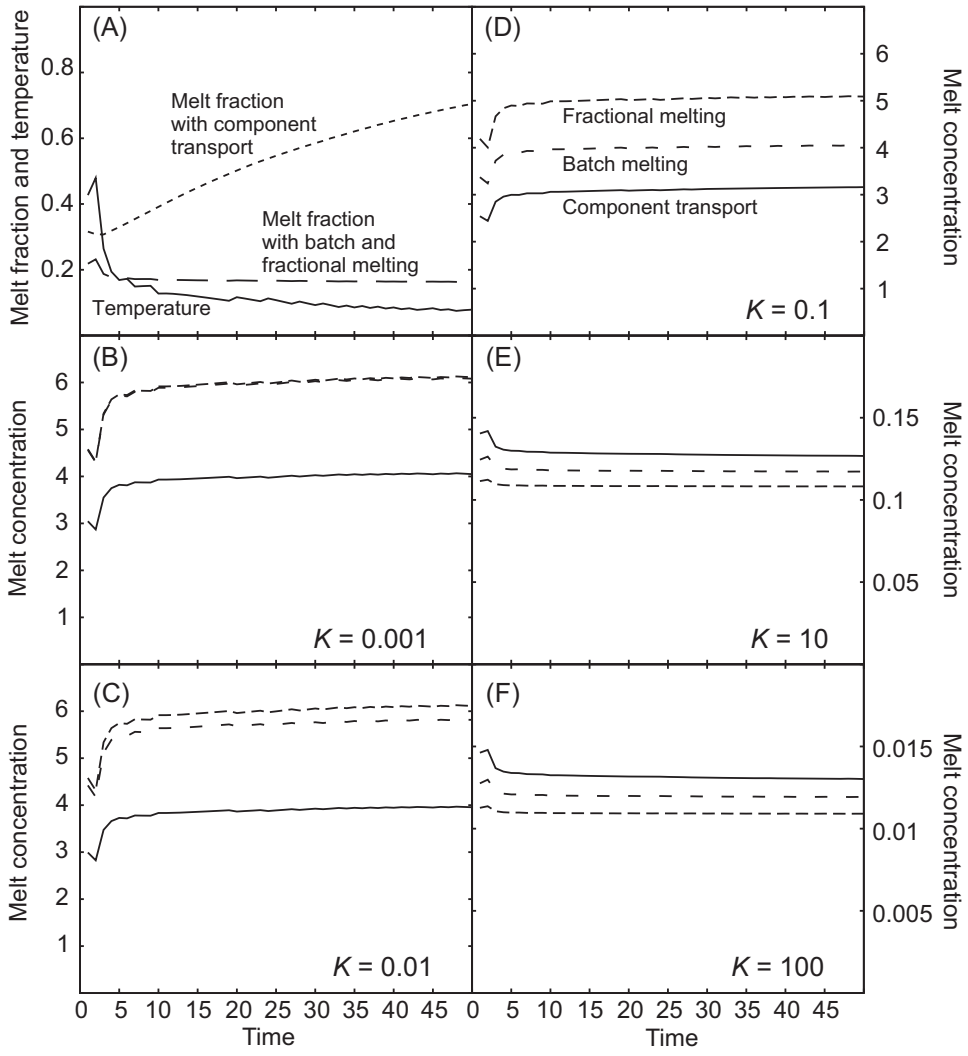

Fig. 12. Time dependency of (A) peak melt fraction and temperature, and (B-F) melt concentration at peak melt fraction, for an initially homogeneous column with uniform trace element distribution $I_i = 1$, for both incompatible ($K < 1$) and compatible ($K > 1$) trace elements. Melting is governed by the eutectic phase diagram; the results shown here were extracted from figure 9. Peak melt fraction occurs at the location of the high melt fraction layer that forms in response to compaction. Also shown are the corresponding results assuming batch (dotted lines) and fractional (dashed lines) melting. These are calculated during melting to the same temperature as the peak melt fraction in the melt layer; this temperature is shown in (A).

given major element concentration had been obtained by batch or fractional melting, consistent with the results obtained in the previous section.

Constant Initial Temperature with Cooling from Above and Below in an Initially Homogenous Column

The final dimensionless results are for a homogenous column with initial conditions $T_i = \phi_i = 0.6$, $C_i = 0.2$ and $I_i = 1$, governed by the eutectic phase diagram, which is cooled from above and below by fixing the temperature $T = -0.3$ (that is, at a

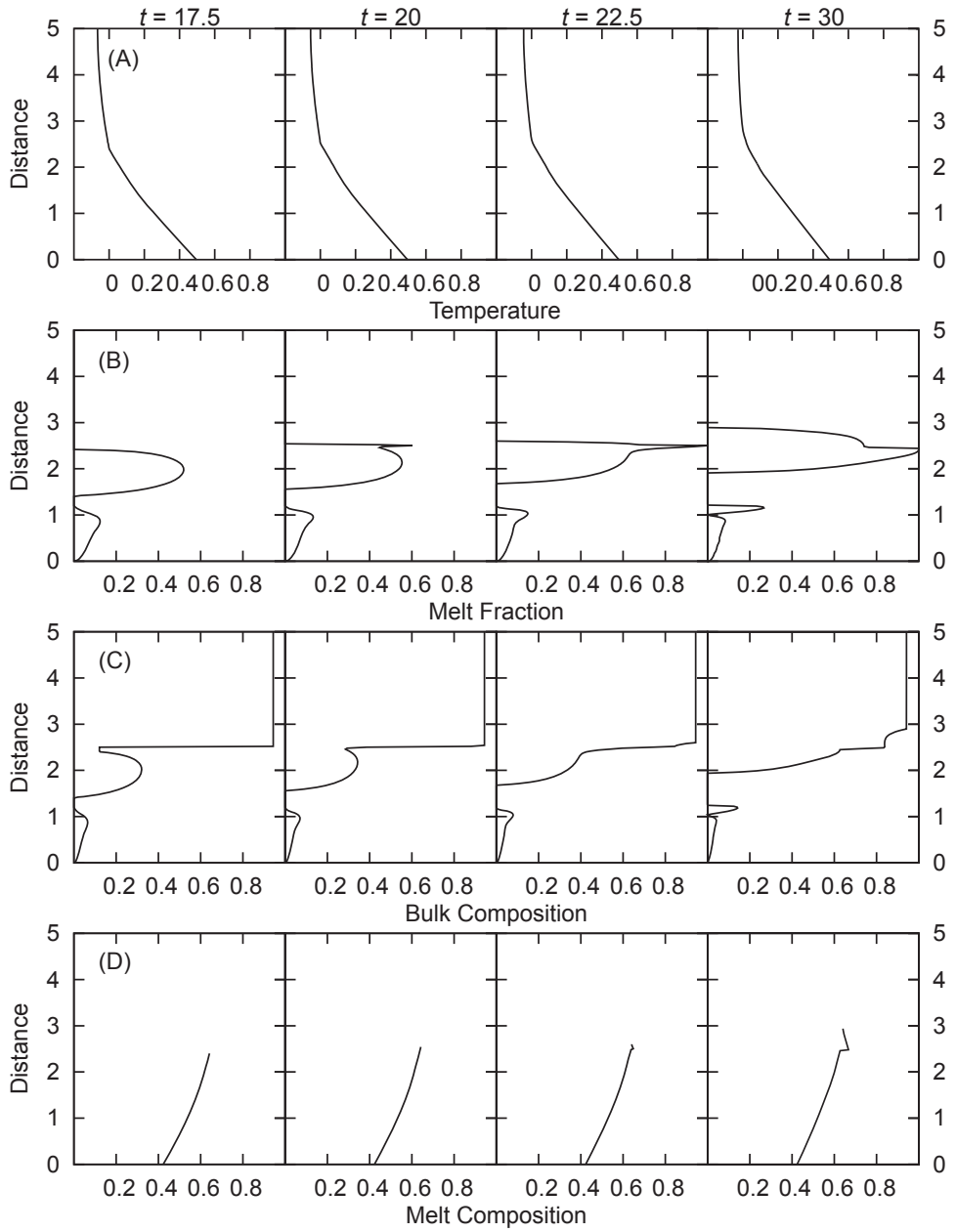

Fig. 13. (A) Temperature, (B) melt fraction, (C) bulk composition and (D) melt composition at t = 17.5, 20, 22.5 and 30, for an initially heterogeneous column with $T_i = -0.1$ and $\phi_i = 0$, governed by the eutectic phase diagram (fig. 2A). The initial bulk composition is the same as that shown in figure 8. The column is heated from below with $T_{z=0} = 0.5$ for all time. Time-steps are not equally spaced, to show the behavior after the upper layer begins to melt. The solid composition is not shown, and is constant at $C = 0$ (pure component A) in the partially molten zone in the lower layer (where $z < 5$ and $T > T_S$), constant at $C = 1$ (pure component B) in the partially molten zone in the upper layer (where $z \geq 5$ and $T > T_S$) and at the initial composition $C = C_i$ elsewhere.

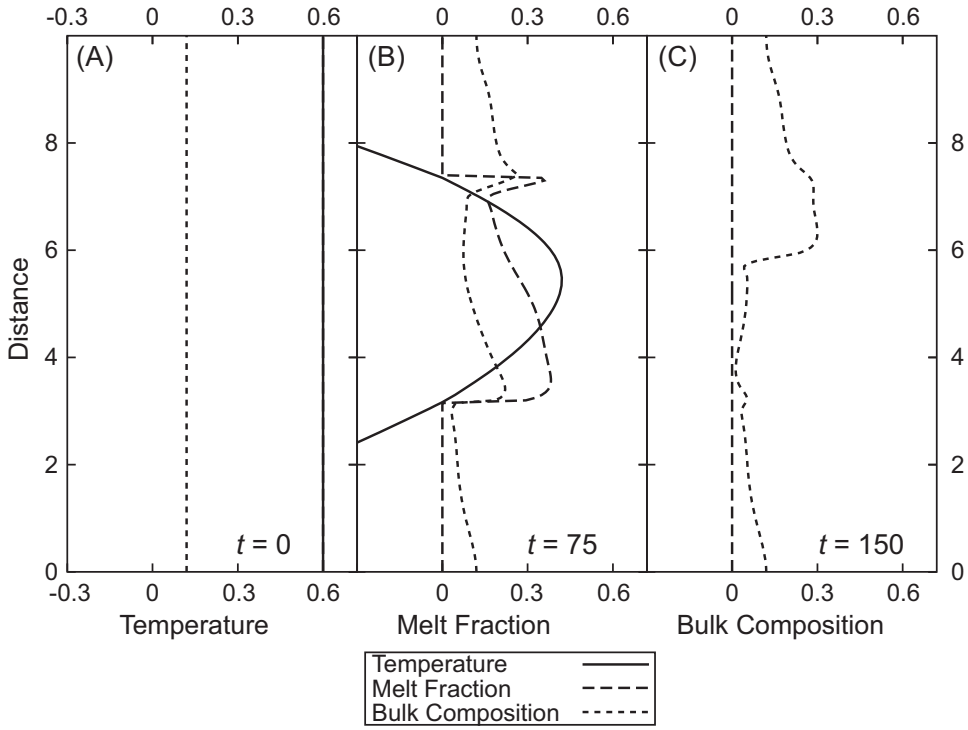

Fig. 14. Temperature, melt fraction and bulk composition at $t = 0$, 75 and 150 for an initially homogeneous column with $T_i = \phi_i = 0.6$ and $C_i = 0.2$, governed by the eutectic phase diagram (fig. 2A). The column is cooled from above and below, with $T_{z=0} = T_z = z_{Mi} = -0.6$ for all time. The temperature curve is not observed in (C) at $t = 150$ because the column has cooled below $T = -0.5$. The column is entirely solid at this time, and the resulting bulk composition is frozen in place.

temperature below the solidus $T = 0$) at the upper and lower boundaries (fig. 1E). At $t = 0$, the column contains 40 percent crystals, representing magma emplaced as a slurry, or emplaced as a liquid that cools rapidly by convection to form a slurry, after which convection is inhibited (figs. 14A and 14B). During the subsequent evolution of the mush, melt migration and component transport lead to variations in the local bulk composition: upwards migration of melt leads to enrichment of B at the top of the column, where there is a net accumulation of melt, and enrichment in A at the base of the column (fig. 14B). By $t = 150$, the column has cooled below the solidus temperature, so there is no melt present (fig. 14C). Trace element concentrations frozen in place at this time are shown in figure 15. Incompatible trace elements accumulate at the top the column, transported there by the migrating melt, and are depleted at the base (fig. 15A); compatible elements accumulate at the base of the column and are depleted at the top (fig. 15B). Regions in which melt migration has had a significant impact on concentration are those that show a large change from the initial trace element concentration ($I_i = 1$). The spatial distribution of trace elements also depends on the partition coefficient, with incompatible elements showing deviations of larger amplitude from $I_i = 1$ with decreasing K, and compatible elements showing deviations of larger amplitude but smaller vertical extent with increasing K.

DISCUSSION

Our results suggest that component transport and chemical reaction plays an important role in the evolution of a crystalline mush undergoing buoyancy-driven

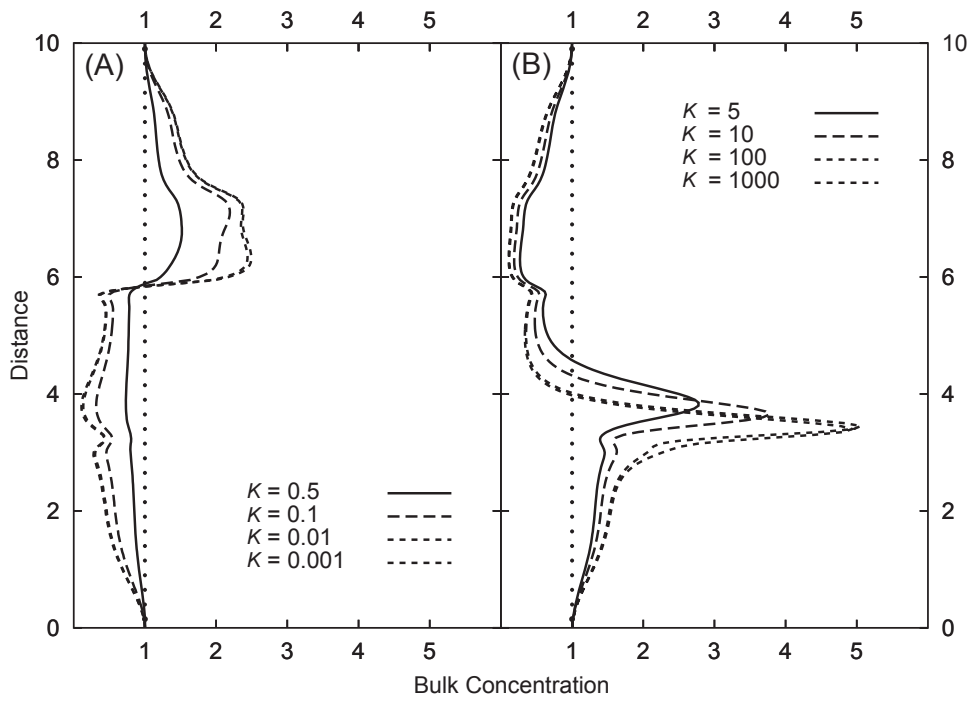

Fig. 15. Bulk trace element concentrations at $t = 150$, for both incompatible ($K < 1$) and compatible ($K > 1$) trace elements in the column shown in figure 14, cooled from above and below. The column is entirely solid at this time, and the resulting trace element concentrations are frozen in place.

compaction, producing compositional variation in both major and trace elements that is not captured by existing models. The decoupling of major and trace elements is a key finding. Even for the simplest case of a homogenous, insulated column that is instantaneously melted then allowed to compact, component transport leads to spatial variations in major element composition as melt migrates through, and reacts with, the crystalline mush; moreover, component transport changes the trace element composition of the melt that leaves the mush, producing melt that is more enriched in incompatible elements than predicted by a batch melting model. More strikingly, in a two-layer column governed by a eutectic phase diagram, mixing of upwards-migrating melt and downwards-migrating solid at the interface between compositionally different layers yields a layer of high melt fraction (or even pure melt), with a near-eutectic composition. Models that neglect component transport fail to capture these phenomena, which demonstrates that any model of melting or crystallization that includes relative motion of the melt and solid phases (that is in which melt fraction changes in response to the motion of melt or crystals) must account for changes in local bulk composition when describing local phase equilibria. Most previous studies have assumed that melting or crystallization in an initially homogeneous system can be modeled using, for example, a single suite of temperature-phase fraction curves, obtained either experimentally, or using a program such as MELTS, for the given starting bulk composition (see, for example, fig. 5 in Gutierrez and Parada, 2010). This suite of curves is then applied at all locations and for all time, even though the local bulk composition and, hence, the local phase relations, are modified by the relative motion of melt and solid during melt percolation or crystal settling (for example

Fountain and others, 1989; Jackson and Cheadle, 1998; Tharp and others, 1998; Boudreau and Philpotts, 2002; Jackson and others, 2003, 2005; Gutierrez and Parada, 2010; Solano and others, 2012). Such an approach ignores the impact of component transport on local bulk composition. Properly accounting for phase transport requires the use of multiple suites of temperature-phase fraction curves, each corresponding to a local bulk composition that changes through time. This is one reason why we use here a simple approach to phase equilibria, rather than a more complex approach involving, for example, MELTS; calculating phase equilibria in a system where local bulk composition changes with time is trivial using a simple phase diagram, but computationally intensive using a program such as MELTS.

In models heated from below, a high porosity layer forms as melt migrates upwards more rapidly than heat, and accumulates at the top of the partially molten region. Several studies have observed similar behavior (for example, Jackson and Cheadle, 1998; Jackson and others, 2003), but here we demonstrate that the melt in the high porosity layer has a major element composition corresponding to only a small fraction of batch (static) melting (that is, it is close to the eutectic composition for a eutectic phase diagram, and enriched in the low temperature component for a solid-solution phase diagram), despite occupying a high melt fraction. The reason is that the melt has migrated into, and locally equilibrated with, mush at low temperature. Moreover, the melt in the high porosity layer is less enriched in incompatible trace elements than would be observed if melt with the same bulk composition had been produced by batch or fractional melting. We discuss the implications of these results for crustal differentiation in the next sections; here we simply note that models that aim to explain the evolution of heterogeneous multi-component systems must account for component transport.

The parameters governing compaction, particularly the value of the key dimensionless parameter κ_{eff}, will vary from one magmatic situation to another. The effect of varying the value of κ_{eff} on melt migration in systems heated from below has been investigated previously (Jackson and Cheadle, 1998; Jackson and others, 2003) and a repeat of their work is outside the scope of the current study. However, our results and conclusions are not unique to the value of κ_{eff} used. Figure 16 shows melt fraction and bulk composition at a single snapshot in time, during heating from below of the same eutectic system modeled previously but with $C_i = 0.2$, for values of κ_{eff} varying over the four orders of magnitude predicted for crustal igneous systems. Smaller values of κ_{eff} yield thinner melt layers, located closer to the base of the column; larger values yield higher melt fractions and thicker melt layers. However, we observe the same pattern of enrichment in B ($C = 1$) in the melt layer where there is a net accumulation of melt, and depletion in B at the base of the column where there is net loss of melt, regardless of the value of κ_{eff}. The effect of component transport on bulk and melt composition is similar, regardless of the value of κ_{eff}. We also expect similar results for ternary and quaternary phase diagrams that are more complex than the simple binary systems considered here, but better represent real rocks (Weill and others, 1980). Component transport will lead to local variations in bulk composition, causing phase change and associated temperature change, regardless of how many components are present. Mixing between melt and solid in disequilibrium will yield high melt fraction in any system with a eutectic composition.

Formation of Evolved Magmas in Deep Crustal Hot Zones

There is abundant geological, geochemical and geophysical evidence to suggest that chemical differentiation occurs at depth in the crust, and that the middle and lower crust may be the dominant source of evolved magmas in regions termed Deep Crustal Hot Zones (DCHZ; Annen and others, 2006) or Melting-Assimilation-Storage-Hybridization (MASH) zones (Hildreth and Moorbath, 1988). Numerous thermal

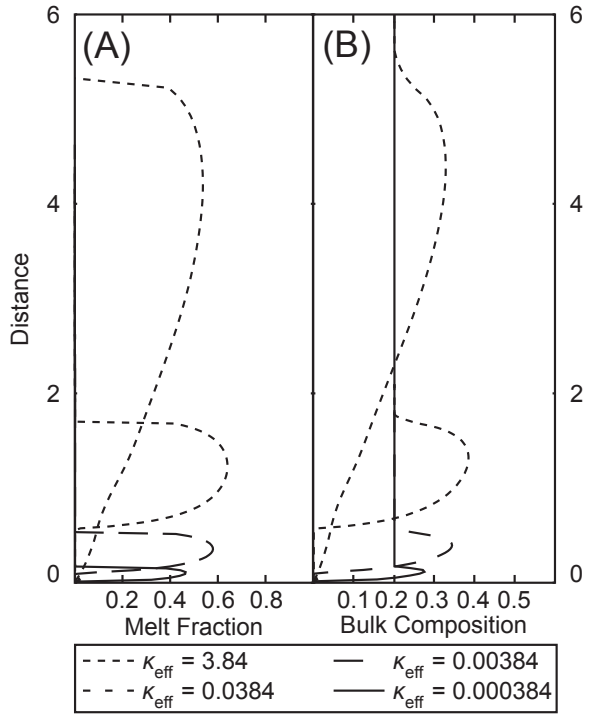

Fig. 16. (A) Melt fraction and (B) bulk composition at $t = 25$, for a range of values of the key dimensionless scaling parameter κ_{eff}, typical of crustal igneous systems. The column is initially homogeneous, with $T_i = -0.1$, $\phi_i = 0$ and $C_i = 0.2$; melting is governed by the eutectic phase diagram (fig. 2A). The column is heated from below, with $T_{z=0} = 0.5$ for all time.

models have demonstrated that the intrusion of hot, mantle-derived primary magma into the lower crust can produce large volumes of partial melt, either by heating and melting of the crust, or cooling and crystallization of the intruded basalt (for example, Hodge, 1974; Huppert and Sparks, 1988; Bergantz, 1989; Bergantz and Dawes, 1994; Petford and Gallagher, 2001; Annen and Sparks, 2002; Dufek and Bergantz, 2005; Annen and others, 2006). However, few studies have investigated the mechanisms by which melt generated in this way segregates from its partially molten host. Jackson and others (2003) and Solano and others (2012) argued that the DCHZ is in a mush state for most of its life, except when a new influx of basaltic magma generates a transient magma chamber. Partial melt in the mush migrates upwards along grain boundaries, and accumulates near the top of the DCHZ, forming one or more high porosity layers similar to those observed here. The melt fraction accumulates until it reaches the "solid-to-liquid" transition [SLT of Rosenberg and Handy (2005) or the "critical melt fraction" (CMF) of van der Molen and Paterson (1979)], at which point the mush disaggregates yielding a mobile magma ("slurry") comprising melt and suspended crystals. Such a melt-rich layer is unlikely to be stable, and the magma will ascend to higher crustal levels via dikes, faults or fractures to erupt directly, or form upper crustal magma chambers and plutons (for example Grosfils, 2007; Karlstrom and others, 2009, 2010). Jackson and others (2003, 2005) also argued that the melt in the high porosity layer is chemically evolved, because it has equilibrated with solid at low temperatures near the top of the DCHZ. Thus, the coupled processes of melt migration and chemical reaction through a temperature gradient give rise to evolved

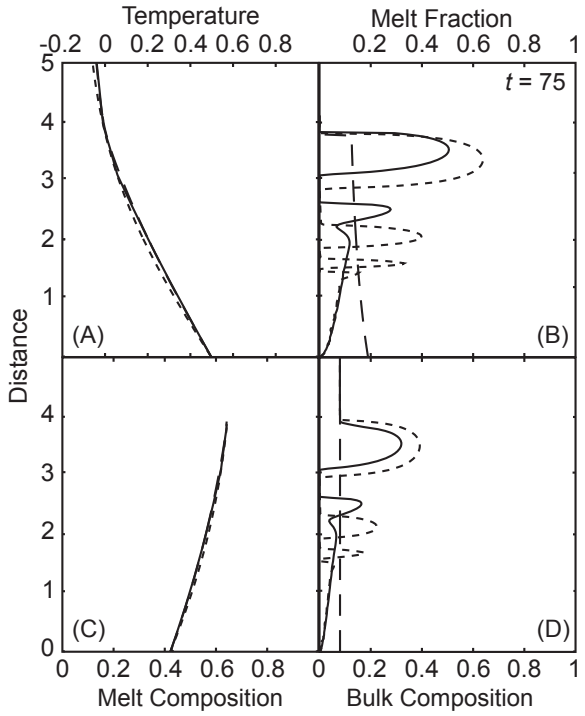

Fig. 17. (A) Temperature, (B) melt fraction, (C) melt composition and (D) bulk composition at $t = 75$, for an initially homogeneous column with $T_i = -0.1$, $\phi_i = 0$ and $C_i = 0.08$, governed by the eutectic phase diagram (fig. 2A). The column is heated from below with $T_{z=0} = 0.5$ for all time. Solid lines show results with melt migration and component transport (the model presented here); dotted lines show results with melt migration but no component transport (that is, phase behavior is predicted assuming constant bulk composition and the model presented by Jackson and Cheadle, 1998 and Jackson and others, 2003, 2005); dashed lines show results assuming no melt migration (thermal models presented by numerous authors, including Hodge, 1974; Bergantz, 1989; Petford and Gallagher, 2001; and Annen and Sparks, 2002).

magma in DCHZ. However, Jackson and co-workers (Jackson and Cheadle, 1998; Jackson and others, 2003, 2005; Solano and others, 2012) used experimental data to describe phase change and melt composition for a given temperature and initial bulk composition. As we show here, melt migration changes the local bulk composition, invalidating the use of empirical phase equilibrium data obtained for a single bulk composition. Jackson and co-workers also assumed a uniform initial crustal composition, and did not model trace element transport.

We compare the model predictions of Jackson and co-workers, with our model in which component transport is included, using the same eutectic phase diagram as before but with an initial bulk composition $C_i = 0.08$, and assuming heating from below (fig. 17). We also consider the case where there is no melt migration, corresponding to numerous previous thermal models (for example, Hodge, 1974; Huppert and Sparks, 1988; Bergantz, 1989; Bergantz and Dawes, 1994; Petford and Gallagher, 2001; Annen and Sparks, 2002; Annen and others, 2006). Temperature profiles are similar regardless of whether melt and component transport is included (fig. 15A), consistent with Jackson and Cheadle (1998) who found that heat transfer is dominated by conduction for most values of κ_{eff}. Melt composition is also similar, so long as melt migration is modeled (fig. 17C), regardless of whether component transport (resulting in changes in local bulk composition) is included (solid line; model presented here) or

excluded (dotted line; model of Jackson and co-workers). However, component transport has a significant impact on melt fraction and (local) bulk composition; melt fractions are generally lower when component transport is included (compare solid and dotted lines in fig. 17B) and, as a result, the bulk composition is less enriched in B (fig. 17D). Models that omit melt migration predict uniform compositions and a melt fraction that simply decreases upwards, falling to zero at the solidus isotherm (dashed lines in fig. 17).

As discussed above, the composition of the melt in the high porosity layer corresponds to only a small fraction of batch (static) melting (that is, it is close to the eutectic composition) regardless of whether component transport is included, confirming the assumption of Jackson and co-workers that melt in the high porosity layer is chemically evolved because it has equilibrated with solid at low temperatures. However, melt fractions are lower when component transport is included, because the decreasing fertility of the mush is accounted for as melting proceeds. As melt migrates upwards, the remaining mush becomes increasingly enriched in A and, therefore, more refractory. If component transport is not accounted for, this behavior is not captured and the base of the column continues to produce melt. Our findings confirm the predictions of Jackson and co-workers (Jackson and Cheadle, 1998; Jackson and others, 2003, 2005; Solano and others, 2012) that melt segregation and component transfer in DCHZ will give rise to evolved magmas, as melt migrates upwards and equilibrates with matrix at low temperature. However, the model of Jackson and co-workers fails to account for the decreasing fertility of the protolith. The results presented here also suggest that evolved magmas can form at the interface between layers of contrasting composition (figs. 8 and 13). This has not been suggested previously, because it is only predicted by models in which component transport is accounted for. Modeling of multiple compositional layers, rather than the simple pair presented here, gives rise to multiple melt layers, similar to those observed in migmatites. Deformation of the layered protolith could collect this melt in dilatant sites such as shear and boudins, as observed in numerous outcrops (for example, Sawyer, 1991, 1994; Brown, 1994; Brown and others, 1995). Regardless of how it forms, the evolved magma will be less enriched in trace elements than would be expected if the same major element composition had been obtained by batch or fractional melting. This distinctive chemical signature, in which magmas from DCHZ appear to be less fractionated in trace elements than major elements, is a predictive aspect of the model that can be tested against field data.

Application to Natural Lower Crustal Settings: The Mafic Complex of the Ivrea-Verbano Zone

The Ivrea-Verbano zone, Italy, is a section of the middle to lower crust which was uplifted and tilted by about 90° during the Alpine orogeny. Two main units have been identified: the Kinzigite Formation and, of particular interest here, the Mafic Complex (fig. 18). The Mafic Complex is approximately 8 km thick and 35 km wide at the southern end of the Ivrea-Verbano zone, and has been uplifted from a depth of at least 15 km. Deeper levels of the crust are exposed towards the Insubric Line, so a traverse, approximately east-west, increases the depth of formation of the exposed rocks (Zingg, 1990; Henk and others, 1997; Demarchi and others, 1998). Five main units have been identified within the Mafic Complex: the diorites (DIO), the main gabbro (MG) and the upper, intermediate and lower basal zones (UZ, IZ and BZ) (fig. 18). Peressini and others (2007) interpreted two separate phases of magmatism using U-Pb SHRIMP dating of zircons. The first is associated with the regional-scale metamorphism that formed the Kinzigite Formation at 310 Ma; the second is the intrusion of the Mafic Complex between 295 Ma and 285 Ma. Barboza and others (1999) also concluded that the Mafic Complex was intruded after the metamorphism associated with the Kinzigite Formation.

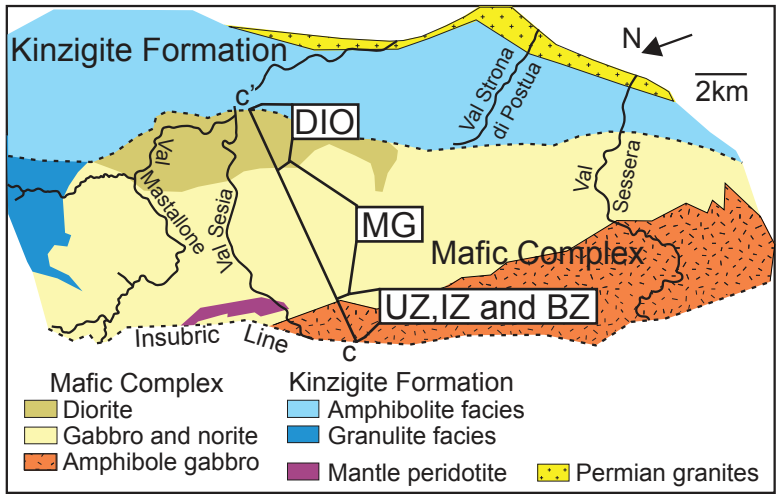

Fig. 18. Simplified geological map of the Mafic Complex in the Ivrea-Verbano zone, showing the main units referred to in the text along the east-west transect labelled C-C′ from paleo-top to paleo-base of the Mafic Complex. Note north is approximately 260° from vertical. BZ denotes Basal Zone, IZ denotes Intermediate Zone, UZ denotes Upper Zone, MG denotes Main Gabbro and DIO denotes Diorite. Modified from Peressini and others (2007).

Quick and co-workers (Quick and others, 1992, 1994, 1995; Sinigoi and others, 1995, 1996) ascribed the formation of the Mafic Complex to repeated intrusion of mantle-derived basalts, which crystallized whilst melting and partially assimilating the surrounding country rock. The basalts periodically replenished a small and transient magma chamber (in the sense that the liquid part any given time was small compared to the total volume of emplaced magma) that progressively accumulated a large thickness of cumulates (a mush zone) at the base. In their model, based on direct field observations, the Mafic Complex was, for the most part, in a mush state prior to full solidification, consistent with our focus here on mush processes. Some of the early intrusions within the BZ cooled before causing melting of the surrounding country rock, so retain their original trace element signatures; paragneisses derived from the roof of the intrusion also became incorporated in the BZ as septa, retaining a crustal signature. However, heat released by the intruding magmas eventually caused partial melting in the roof, and in the septa interleaved with the intrusions, while buoyancy drove the upwards migration of evolved ("granitic" in the broad sense) melt through the mush. This migration of melt lead to (i) mixing of mantle-derived magma with crustal melts and the formation of hybrid melts, (ii) local accumulation of evolved melts and associated incompatible elements in the upper Mafic Complex and overlying roof, and (iii) depletion of the septa in incompatible elements. Neodymium and strontium isotope data suggest that hybridization with lower crustal melts occurred throughout (Voshage and others, 1990).

Motivated by the observations of Quick and co-workers (Quick and others, 1992, 1994, 1995; Sinigoi and others, 1995, 1996), we focus here on modelling buoyancy-driven melt flow and chemical reaction within the mushy magma chamber and partially molten crust. We model the repetitive emplacement of mantle-derived basaltic magmas and subsequent migration of melt in a simple, vertically oriented, 1D model, to investigate whether trace element transport during melt migration can lead to the observed trace element distribution within the Mafic Complex. Model parameters are summarized in table 3, and are used to present the results in dimensional form;

Table 3

Material properties used to produce the dimensional results shown in figure 19

Symbol	Description	Value	Source
a	grain size	2.5mm	Jackson and others (2003)
b	permeability constant	0.002	Jackson and others (2003)
c_P	Specific heat capacity	1100J kg^{-1} K^{-1}	Peressini and others (2007)
C_i	Initial composition	0.8	assumed
I_{icrust}	crustal Nd concentration	35ppm	Voschage and others (1990)
$I_{ibasalt}$	basalt Nd concentration	8ppm	Voschage and others (1990)
k_T	thermal conductivity	3W K^{-1} m^{-1}	Peressini and others (2007)
K	Nd partition coefficient	0.087	Voschage and others (1990)
L_f	latent heat of fusion	550000J·kg^{-1}	Peressini and others (2007)
Ste	Stefan number	0.64	equation (35)
T_{geo}	geothermal gradient	25K·km^{-1}	Peressini and others (2007)
T_L	solidus temperature	1426K	Peressini and others (2007)
T_S	liquidus temperature	1147K	Peressini and others (2007)
η	matrix bulk viscosity	10^{16}Pa·s	Jackson and others (2003)
κ_{eff}	effective thermal diffusivity	0.48	equation (34)
μ	melt shear viscosity	10^{4}Pa·s	Jackson and others (2003)
ρ	density	2800kg·m^{-3}	Peressini and others (2007)
$\Delta\rho$	solid-melt density difference	500 kg·m^{-3}	Jackson and others (2003)
ξ	matrix shear viscosity	10^{16}Pa·s	Jackson and others (2003)

no attempt is made to adjust the parameters to better match the observed data. Trace element parameters are from Voshage and others (1990), while thermal parameters are from Peressini and others (2007). Parameters governing compaction and melt transport are from Jackson and others (2003). Modeling of the processes which cause the observed trace element distribution within the Mafic Complex has not previously been attempted, but it has been suggested that trace element concentrations in all units lie on mixing lines between crust and primary magma, and assimilation-fractional-crystallization (AFC) models have been used to model trace element concentrations, assuming these vary only by the amount of mixing (assimilation) between crust and primary magma (Voschage and others, 1990). No explicit tracking of trace element migration associated with melt flow has been attempted.

Peressini and others (2007) modeled the thermal consequences of emplacing a single, 8 km thick layer of basalt (that is, corresponding to the thickness of Mafic Complex) into the lower crust, at a depth of 18 km, to investigate the time required to reach the closure temperature of the Sm-Nd system. However, a single emplacement event of this thickness is unrealistic so, following the approach of Solano and others (2012), we model the repeated intrusion of 200 m thick layers of basalt every 40 ka (at a time-averaged rate of 5 mm $\cdot$ a^{-1}), to produce the total of 8 km over a time period of 1.6 Ma. The sills are intruded at the liquidus temperature of 1150 °C into crust with a pre-existing geothermal gradient of 25 °C $\cdot$ km^{-1}. To model the septa of country rock observed in the field, sills are not emplaced at a fixed depth; instead, they are randomly emplaced in a region 400 m wide, centred at a depth of 18 km. The eutectic phase diagram employed previously is used to approximate the melt fraction versus temperature relationship of basaltic magmas, but with $c_1 = 1426.15$ and $c_2 = 875.25$ (eqs 13, 14) to match the solidus and liquidus temperatures used by Peressini and others (2007).

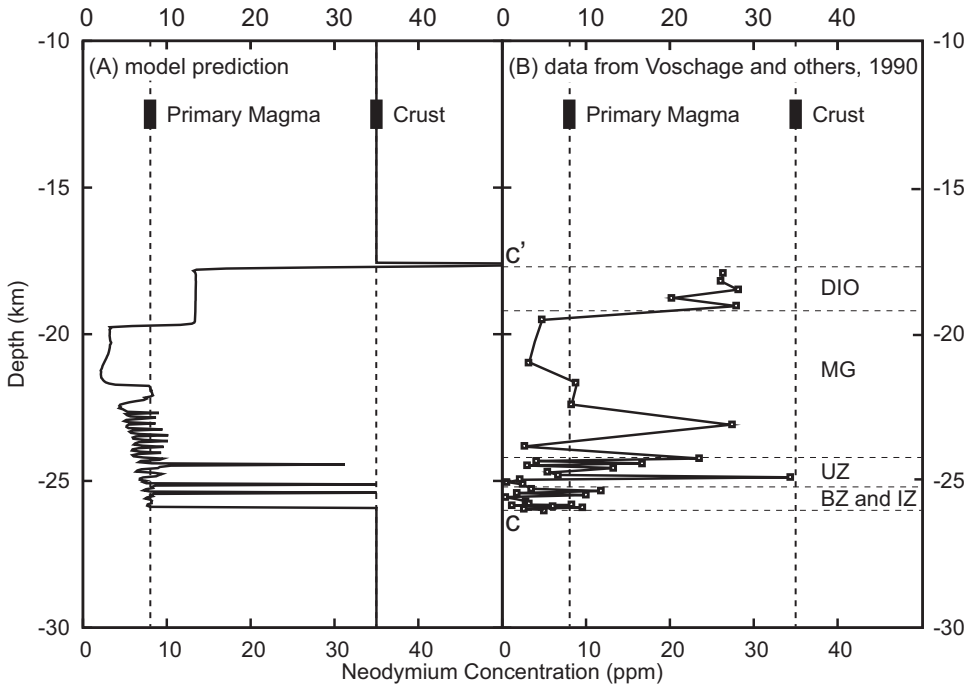

Fig. 19. Comparison between modeled and measured neodymium bulk concentrations along the transect C-C' shown in figure 18. Vertical dashed lines show neodymium concentrations in the primary magma and crust; horizontal dashed lines show the boundaries between the basal zone (BZ), intermediate zone (IZ), upper zone (UZ), main gabbro (MG) and diorite (DIO). Measured data and geological zone boundaries are from Voshage and others (1990).

Figure 19 compares the model predictions against Nd concentrations measured along a 1-D traverse, oriented approximately east-west (that is, from paleo-top to base), through the Mafic Complex (Voshage and others, 1990). In both modeled and measured data, the BZ and IZ are characterized by significant variations in Nd concentration, with the upper values approaching the assumed crustal concentration. The UZ and lower part of the MG also exhibit variations in Nd concentration, but these are generally smaller in magnitude than those observed in the BZ and IZ. The upper part of the MG is depleted in Nd relative to the initial primary magma, while the DIO is significantly enriched in Nd relative to the initial primary magma, and the upper part of the underlying MG. Significant melt migration can occur only when melt is present in the period between intrusions, which requires sufficient heat to have been transferred into the system (Solano and others, 2012). Consequently, in the BZ and IZ, variations in Nd concentration are dominated by the alternating layers of unmelted septa and intruded basalt, which cooled and crystallised without interacting with the septa. This behavior is captured by a model of repeated intrusion, but not by models that assume a single, large magma pulse (for example, Perissini and others, 2007). In the UZ and the lower part of the MG, variations in Nd concentration between septa and intruded basalt are less pronounced, because sufficient heat has been transferred into the system to allow partial melting of the septa and, therefore, melt migration occurs within and between the septa and the intruded basalt. In the upper part of the MG, variations in Nd concentration between basalt and septa are not preserved, because the latter have been entirely assimilated. The upper part of the MG is depleted

in Nd, because melt has migrated upwards and accumulated in the DIO, which as a result, is enriched in Nd. This behavior is only captured by a model that includes component transport. The model also predicts a very high Nd concentration in the crust immediately above the Mafic Zone, where partial melting of the crust has occurred and Nd-rich melt has accumulated. However, there are no field data available to confirm this prediction.

The trace element distribution predicted by a model that includes repeated intrusion of basalt and component transport associated with melt migration through a compacting, crystalline mush, produces a reasonable match to the observed data (fig. 19). Repeated intrusion leads to interleaved septa with a crustal signature, and intruded sills with a primary magma signature, in the BZ and IZ, whilst melt migration leads to depletion of the upper part of the MG and enrichment of the overlying DIO. Moreover, melt migration and differentiation occurs over timescales consistent with the thermal budget associated with emplacement of the observed volume of mafic magma. A reasonable match between the model predictions and measured data is the best that should be expected given the simplistic model assumptions, including (i) constant sill thickness and emplacement rate, with poorly constrained values for both of these parameters, (ii) constant material properties such as melt viscosity, and (iii) use of a simple binary phase diagram to describe melting. Nevertheless, the results suggest that melt migration and coupled trace element transport provides a mechanism to explain the observed variation in Nd concentration in a DCHZ such as the Mafic Complex, consistent with thermal budgets and timescales. Moreover, they support key aspects of the field-based model of Quick and co-workers (Quick and others, 1992, 1994, 1995; Sinigoi and others, 1995, 1996), including (i) formation of the Mafic Complex by repeated intrusion of basaltic sills, (ii) the presence of a small, transient, liquid magma chamber and a large, cumulate pile, (iii) the importance of buoyancy-driven melt flow along grain boundaries leading to mixing of mantle and crustal melts, and (iv) the buoyancy-driven accumulation of evolved (granitic, in the broad sense) melt in the Mafic Zone and overlying roof.

Application to Natural Upper Crustal Settings: The Rum Layered Intrusion

Melt migration within the cumulate pile has been suggested as a mechanism for some of the observed differentiation in layered igneous intrusions (for example, Irvine, 1980; Naslund and McBirney, 1996). The Rum layered intrusion in Scotland has been mapped extensively and shows evidence for post-cumulate melt migration. Of particular interest here is the so-called "Wavy Horizon" of Unit 9 (Bédard and others, 1988; Holness and others, 2007), a pyroxene-rich layer at the contact between an underlying troctolite, consisting primarily of olivine and plagioclase with small amounts of pyroxene, and an overlying gabbro (fig. 20). The lower contact of the Wavy Horizon undulates across the outcrop, cross-cutting the textural and modal layering (Holness and others, 2007). The formation of the Wavy Horizon has been attributed to the intrusion of a hot, picrite (Mg-rich basalt) sill into a gabbroic cumulate pile, and subsequent infiltration metasomatism (Holness and others, 2007). In this conceptual model, heat and melt from the picrite entered the overlying gabbro, displacing the pre-existing melt and dissolving pyroxene, whilst crystallizing olivine and plagioclase. The pyroxene-rich melt migrated upwards and accumulated to form a melt layer, which then cooled and crystallized prior to further migration, to be preserved in-situ. No quantitative model has yet been presented to support this interpretation, and our aim here is to investigate whether melt migration in an initially homogeneous column can lead to the formation of melt-rich layers similar to the Wavy Horizon.

We present a highly simplified model, in which intrusion of a picrite sill into the gabbro is represented by an initially solid, homogenous column (the gabbro) that is heated from below (the sill). The heat source is then removed and the column is

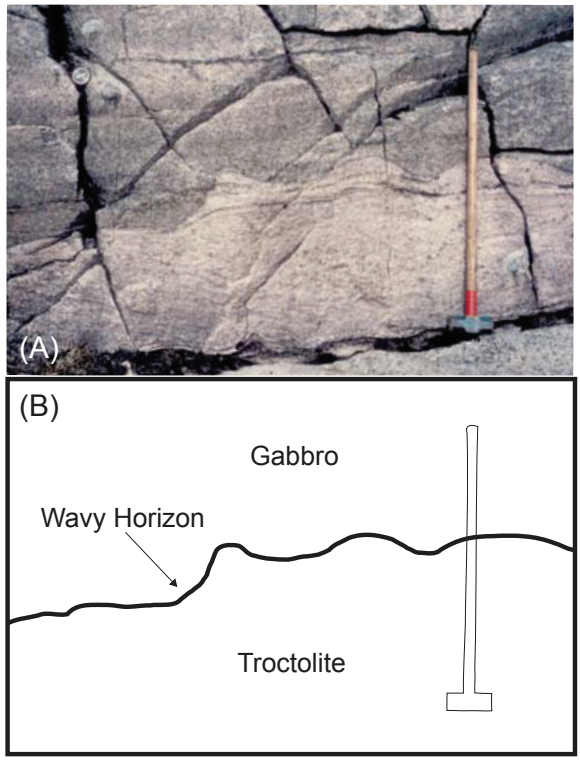

Fig. 20. The Wavy Horizon within Unit 9 of the Rum Layered Intrusion: (A) shows a photograph of part of the outcrop; (B) shows a schematic indicating the troctolite and overlying gabbro, separated by the green, pyroxene-rich Wavy Horizon.

allowed to cool from above and below. Heat and mass transfer is modeled in one-dimension, as melt migration is interpreted to be primarily vertical, although undulations in the Wavy Horizon suggest lateral flow, or lateral variations in vertical flow, were also present. We simplify the Forsterite-Diopside-Anorthite phase diagram by assuming that olivine and plagioclase behave as a single, high-temperature component, and describe phase change using the Forsterite-Diopside binary (Osborne and Tait, 1952). The phase diagram is described using equations (13) and (14), with $a_1 = -128$, $a_2 = -505.55$, $b_1 = -24$, $b_2 = 1143.6$, $c_1 = 1392$, $c_2 = 1251.95$ and $e = 0.125$. The initial composition of the column is $C_i = 0.8$ which, if plagioclase and olivine are treated as one component (Fo), and pyroxene is represented by the other component (Di), corresponds to the bulk composition of the Unit 9 gabbro. Melt at temperatures close to the solidus in the Fo-Di system is highly enriched in Di, owing to the position of the eutectic. We do not attempt to adjust κ_{eff} to match the length- and inferred time-scales for the formation of the Wavy Horizon; the value used is given in table 2. Rather, we qualitatively compare the dimensionless results we obtain from the model with measured data from Holness and others (2007).

As heat enters the column from the underlying picrite sill, a high porosity melt layer forms and rises through the partially molten region (figs. 21A and 21C). The composition of this melt layer is highly enriched in Di ($C = 0$) compared to the initial bulk composition. Below the melt layer, the column is highly depleted in Di; above the melt layer, the column maintains its initial composition (figs. 21B and 21D). At $t = 50$

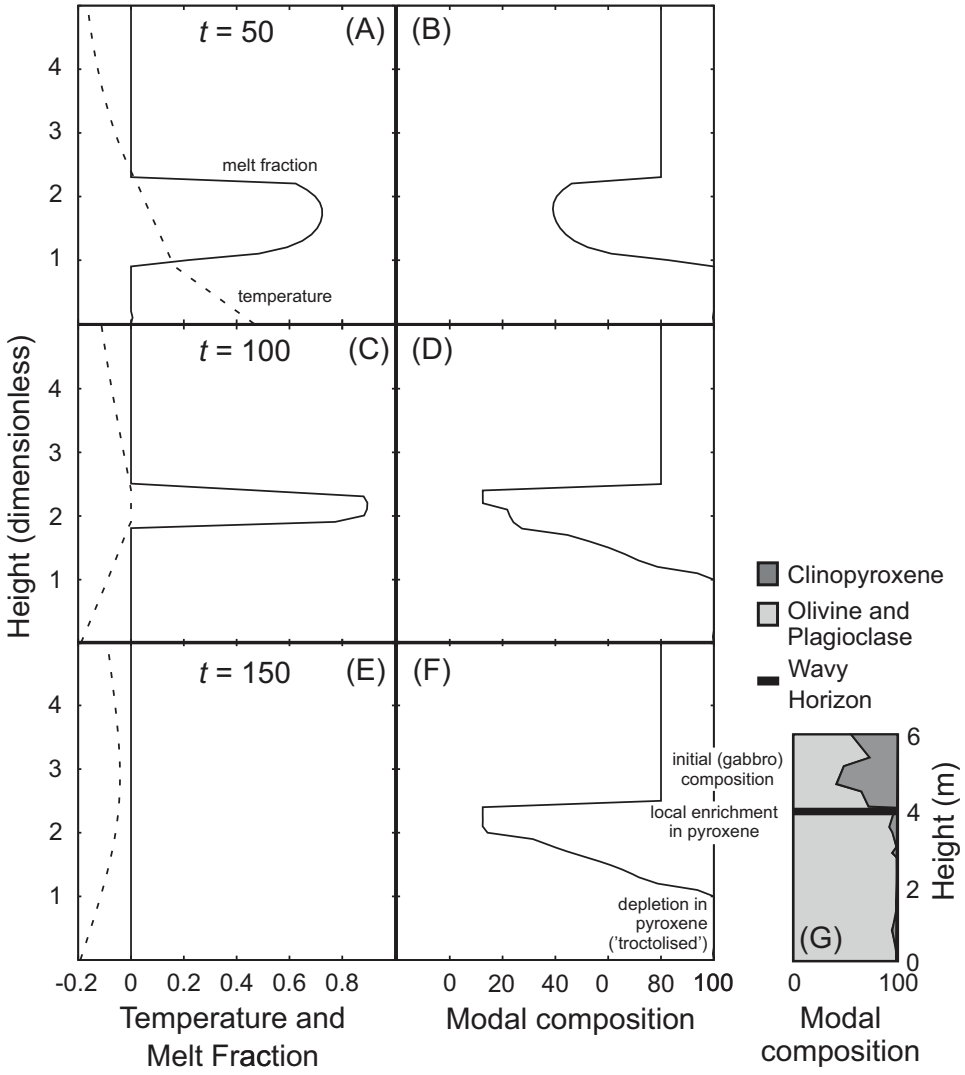

Fig. 21. Temperature, melt fraction and bulk composition for a region with constant initial bulk composition $C_i = 0.8$ at $t = 50$, 100 and 150. The column is initially solid with $T_i = -0.2$, $\phi_i = 0$ and $C_i = 0.8$; melting is caused by heating from below, with $T_{z=0} = 0.5$ until $t = 50$. At this time, heating is stopped and $T_{z=0} = -0.2$. Melting is described by the Forsterite-Diopside binary, and we apply the results to the Wavy Horizon within Unit 9 of the Rum layered intrusion, by assuming that olivine and plagioclase behave as a single component (represented by Fo, and corresponding to $C = 1$) and pyroxene is the other component (represented by Di, and corresponding to $C = 0$). Modal composition through the Wavy Horizon is shown in (g) (data from Holness and others, 2007).

the heat source is removed and the column is allowed to cool, although further heat and mass transfer is allowed; by $t = 150$ the melt layer has frozen (fig. 21E) and the resulting bulk composition is preserved (fig. 21F). The composition at the location of the melt layer is highly enriched in Di, reaching the eutectic value ($C = 0.125$). We argue that this enriched layer is analogous to the Wavy Horizon (fig. 21G), with the bulk composition above corresponding to the gabbro, and the composition below becoming highly depleted in Di, corresponding to the troctolite. As the buoyant melt

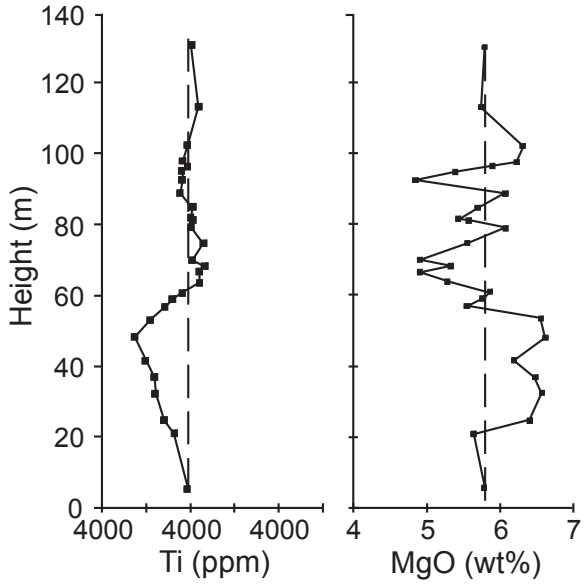

Fig. 22. Magnesium oxide and titanium concentration versus height within the Holyoke flood basalt. Data from Philpotts and others (1996).

migrates upwards, Di (pyroxene) is "washed out" and accumulates in the melt layer. Although simple, the model results suggest that buoyancy-driven melt migration and component transport could have generated the compositional heterogeneity observed in this part of Unit 9.

Application to Natural Lava Flows: The Holyoke Flood Basalt

Crystal mushes also form during the cooling of sills and lava flows, and preserved compositions often display a characteristic S-shaped vertical profile (for example, Philpotts and others, 1996; Latypov, 2003 and references therein; fig. 22). Boudreau and Philpotts (2002) modeled this type of profile in the Holyoke flood basalt, using a model of compaction based on McKenzie (1984) and MELTS to determine bulk composition from temperature. Component transport was not explicitly modeled. The results presented here, for an initially homogenous column being cooled from above and below, are a simple representation of a cooling sill or lava flow (figs. 14 and 15). These profiles match, at least qualitatively, those observed in natural systems (for example, fig. 22). Towards the base of the cooling sill or lava flow, there is a net loss of melt as this migrates upwards, leading to enrichment of high temperature components such as MgO, and depletion in incompatible trace elements such as Ti. The opposite is true towards the top of the sill or lava flow, where melt accumulates. Although simple, the model results suggest that buoyancy-driven melt migration and component transport through a compacting, crystalline mush, could have generated the compositional heterogeneity observed in many sills and lava flows.

CONCLUSIONS

We present the first coupled model of heat and mass transfer within a partially molten, crystalline mush, which includes major and trace element transport, chemical reaction, and compaction, and which is applicable to a number of crustal magmatic scenarios. The model results suggest that component transport and chemical reaction

plays an important role in the evolution of a crystalline mush undergoing buoyancy-driven compaction, producing compositional variation in both major and trace elements that is not captured by existing models. We do not claim that the compaction model is uniquely applicable to the natural systems investigated; rather, that reactive melt flow along grain boundaries, coupled with the inevitable thermal gradients found in crustal mushes, leads to significant, and hitherto unpredicted, modifications to major and trace element melt composition that are not captured by the typically invoked batch and fractional melting/crystallization models, or by models that fail to capture the evolution of local bulk composition when calculating local phase equilibria. In particular, we find that

1. Even for the simplest case of a homogenous, insulated column that is instantaneously melted then allowed to compact, component transport leads to spatial variations in major element composition as melt migrates through, and reacts with, the crystalline mush; moreover, component transport changes the trace element composition of the melt that leaves the mush, producing melt that in this case is more enriched in incompatible elements than predicted by a batch melting model.
2. In deep crustal hot zones (DCHZ) created by the repeated intrusion of hot, mantle-derived magmas, a high porosity layer forms if melt migrates upwards more rapidly than heat, and accumulates near the top of the DCHZ. The melt in this layer has a major element composition corresponding to only a small fraction of batch (static) melting, despite occupying such a high melt fraction, because it has migrated into, and locally equilibrated with, mush at low temperature.
3. Melt migration and chemical reaction in heterogeneous crust, initially comprising rocks of contrasting composition, may lead to the rapid formation of high porosity melt layers at the interface between different rock compositions; moreover, the change in melt fraction is highly counter-intuitive because melt fraction increases as temperature decreases, as a consequence of reactive transport changing the local bulk composition. This has not been suggested previously, because it is only predicted by models in which component transport is accounted for. Melting in a layered crustal protolith could produce multiple melt layers, similar to those observed in migmatites. This prediction should be tested against field data.
4. In both (2) and (3), the melt in the high porosity layer(s) is less enriched in incompatible trace elements than predicted if it is assumed that melt with the same major element composition has been produced by batch or fractional melting. This distinctive chemical signature, in which trace elements appear to be less fractionated than major elements, may be characteristic of magmas that originate in deep crustal hot zones, and the model prediction should be tested against field data.
5. Any model of melting or crystallization that includes relative motion of the liquid and solid phases (that is, in which melt fraction changes in response to the motion of melt or crystals) must account for changes in local bulk composition when calculating phase equilibria; it is not sufficient to measure or calculate, for example, temperature-phase fraction diagrams for a single starting composition and assume that these apply throughout the model for all time. By the same token, it is not sufficient to use trace element models that are based upon a single bulk trace element concentration, or a melt fraction that is referenced to such a bulk composition.
6. Application of the model to a number of crustal systems, including the Ivrea-Verbano zone, the Rum layered intrusion, and the Holyoke flood basalt,

suggests that compositional heterogeneity can be explained by buoyancy-driven melt migration and component transport through a reactive crystalline mush.

The model contains a number of restrictions that limit its application to geologic systems, including material properties that remain fixed regardless of composition and temperature, use of a binary phase diagram to model major components, and a single spatial dimension. Future work will focus on rectifying these limitations. However, even the simple model presented here demonstrates that coupling of heat and melt flow with component exchange between solids and melts generates compositional diversity that is distinct from that predicted by the models of magmatic differentiation that are widely used in igneous geochemistry; use of these models to infer magma sources is therefore questionable. The net upwards migration and accumulation of evolved melts in crystal mushes is likely to be an important process in chemical differentiation of any magma body, from the deep crust, through shallow magma chambers, to thick lava flows.

ACKNOWLEDGMENTS

Mike Cheadle suggested that vertical melt migration and chemical reaction could explain the observed compositional variations in Unit 9 of the Rum intrusion in 1996, and he is gratefully acknowledged for sharing this insight at the time during a fieldtrip with MDJ. Funding from the Leverhulme Trust under grant F/00182/AY is gratefully acknowledged. RSJS and JB acknowledge funding by European Research Council Advanced Grants "VOLDIES" and "CRITMAG" respectively. JB also acknowledges a Wolfson Research Merit Award from the Royal Society.

REFERENCES

Albarède, F., 1996, Introduction to geochemical modelling: Cambridge, United Kingdom, Cambridge University Press, 564 p.

Annen, C., 2009, From Plutons to Magma Chambers: Thermal constraints on the accumulation of eruptible silicic magma chambers in the upper crust: Earth and Planetary Science Letters, v. 284, n. 3–4, p. 409–416, http://dx.doi.org/10.1016/j.epsl.2009.05.006

Annen, C., and Sparks, R. S. J., 2002, Effects of repetitive emplacement of basaltic intrusions on thermal evolution and melt generation in the crust: Earth and Planetary Science Letters, v. 203, n. 3–4, p. 937–955, http://dx.doi.org/10.1016/S0012-821X(02)00929-9

Annen, C., Blundy, J. D., and Sparks, R. S. J., 2006, The Genesis of Intermediate and Silicic Magmas in Deep Crustal Hot Zones: Journal of Petrology, v. 47, n. 3, p. 505–539, http://dx.doi.org/10.1093/petrology/egi084

Asimow, P. D., and Ghiorso, M. S., 1998, Algorithmic modifications extending MELTS to calculate subsolidus phase relations: American Mineralogist, v. 83, p. 1127–1132.

Bachmann, O., and Bergantz, G. W., 2004, On the origin of crystal-poor rhyolites: Extracted from batholithic crystal mushes: Journal of Petrology, v. 45, n. 8, p. 1565–1582, http://dx.doi.org/10.1093/petrology/egh019

Barboza, S. A., Bergantz, G. W., and Brown, M., 1999, Regional granulite facies metamorphism in the Ivrea zone: Is the Mafic Complex the smoking gun or a red herring?: Geology, v. 27, n. 5, p. 447–450, http://dx.doi.org/10.1130/0091-7613(1999)027⟨0447:RGFMIT⟩2.3.CO;2

Bédard, J. H., Sparks, R. S. J., Renner, R., Cheadle, M. J., and Hallworth, M. A., 1988, Peridotite sills and metasomatic gabbros in the eastern layered series of the Rum complex: Journal of the Geological Society, v. 145, p. 207, http://dx.doi.org/10.1144/gsjgs.145.2.0207

Bennon, W. D., and Incropera, F. P., 1987, A continuum model for momentum, heat and species transport in binary solid-liquid phase change systems—I. Model formulation: International Journal of Heat and Mass Transfer, v. 30, n. 10, p. 2161–2170, http://dx.doi.org/10.1016/0017-9310(87)90094-9

Bercovici, D., and Ricard, Y., 2003, Energetics of a two-phase model of lithospheric damage, shear localization and plate boundary formation: Geophysics Journal International, v. 152, n. 3, p. 581–596, http://dx.doi.org/10.1046/j.1365-246X.2003.01854.x

Bercovici, D., Ricard, Y., and Schubert, G., 2001, A two-phase model for compaction and damage, part 1: General Theory: Journal of Geophysical Research, v. 106, n. B5, p. 8887–8906, http://dx.doi.org/10.1029/2000JB900430

Bergantz, G. W., 1989, Underplating and partial melting: Implications for melt generation and extraction: Science, v. 245, n. 4922, p. 1093, http://dx.doi.org/10.1126/science.245.4922.1093

Bergantz, G. W., and Dawes, R., 1994, Aspects of magma generation and ascent in continental lithosphere, *in* Ryan, M. P., editor, Magmatic Systems: International Geophysics, v. 57, ch. 13, p. 291–317, http://dx.doi.org/10.1016/S0074-6142(09)60101-7

Boudreau, A., and Philpotts, A. R., 2002, Quantitative modeling of compaction in the Holyoke flood basalt, Hartford Basin, Connecticut: Contributions to Mineralogy and Petrology, v. 144, p. 176–184, http://dx.doi.org/10.1007/s00410-002-0391-4

Bowen, N. L., 1928, The evolution of the igneous rocks: Princeton, New Jersey, Princeton University Press, 334 p., second edition, 1956, New York, Dover.

Brown, M., 1994, The generation, segregation, ascent and emplacement of granitic magma: The migmatite-to-crustally derived granite connection in thickened orogens: Earth Science Reviews, v. 36, n. 1–2, p. 83–130, http://dx.doi.org/10.1016/0012-8252(94)90009-4

Brown, M., Averkin, Y. A., McLellan, E. L., and Sawyer, E. W., 1995, Melt segregation in migmatites: Journal of Geophysical Research, v. 100, n. B8, p. 15,655–15,679, http://dx.doi.org/10.1029/95JB00517

Cashman, K. V., and Blundy, J., 2013, Petrological cannibalism: the chemical and textural consequences of incremental magma body growth: Contributions to Mineralogy and Petrology, v. 166, n. 3, p. 703–729, http://dx.doi.org/10.1007/s00410-013-0895-0

Claiborne, L. L., Miller, C. F., and Wooden, J. L., 2010, Trace element composition of igneous zircon: a thermal and compositional record of the accumulation and evolution of a large silicic batholith, Spirit Mountain, Nevada: Contributions to Mineralogy and Petrology, v. 160, n. 4, p. 511–531, http://dx.doi.org 10.1007/s00410-010-0491-5

Clemens, J. D., and Petford, N., 1999, Granitic melt viscosity and silicic magma dynamics in contrasting tectonic settings: Journal of the Geological Society, v. 156, n. 6, p. 1057, http://dx.doi.org/10.1144/gsjgs.156.6.1057

Coleman, D. S., Gray, W., and Glazner, A. F., 2004, Rethinking the emplacement and evolution of zoned plutons: Geochronologic evidence for incremental assembly of the Tuolumne Intrusive Suite, California: Geology, v. 32, n. 5, p. 433–436, http://dx.doi.org/10.1130/G20220.1

Connolly, J. A. D., and Podladchikov, Y. Y., 1998, Compaction driven fluid flow in viscoelastic rock: Geodinamica Acta, v. 11, n. 23, p. 55, http://dx.doi.org/10.1016/S0985-3111(98)80006-5

De Paolo, D. J., 1981, Trace element and isotopic effects of combined wallrock assimilation and fractional crystallization: Earth and Planetary Science Letters, v. 53, n. 2, p. 189, http://dx.doi.org/10.1016/0012-821X(81)90153-9

Dell'Angelo, L. N., and Tullis, J., 1988, Experimental deformation of partially melted granitic aggregates: Journal of Metamorphic Geology, v. 6, n. 4, p. 495–516, http://dx.doi.org/10.1111/j.1525-1314.1988.tb00436.x

Dell'Angelo, L. N., Tullis, J., and Yund, R. A., 1987, Transition from dislocation creep to melt-enhanced diffusion creep in fine-grained granitic aggregates: Tectonophysics, v. 139, n. 3–4, p. 325–332, http://dx.doi.org/10.1016/0040-1951(87)90107-7

Demarchi, G., Quick, J. E., Sinigoi, S., and Mayer, A., 1998, Pressure gradient and original orientation of a lower-crustal intrusion in the Ivrea-Verbano zone, northern Italy: The Journal of Geology, v. 106, n. 5, p. 609–621, http://dx.doi.org/10.1086/516045

Dufek, J., and Bergantz, G. W., 2005, Lower Crustal Magma Genesis and Preservation: a Stochastic Framework for the Evaluation of Basalt–Crust Interaction: Journal of Petrology, 46, n. 11, p. 2167–2195, http://dx.doi.org/10.1093/petrology/egi049

Fountain, J. C., Hodge, D. S., and Shaw, R. P., 1989, Melt segregation in anatectic granites: A thermo-mechanical model: Journal of Volcanology and Geothermal Research, v. 39, n. 4, p. 279–296, http://dx.doi.org/10.1016/0377-0273(89)90093-0

Freer, R., 1981, Diffusion in silicate minerals and glasses: A data digest and guide to the literature: Contributions to Mineralogy and Petrology, v. 76, n. 4, p. 440–454, http://dx.doi.org/10.1007/BF00371486

Getsinger, A., Rushmer, T., Jackson, M. D., and Baker, D., 2009, Generating High Mg-numbers and Chemical Diversity in Tonalite-Trondhjemite-Granodiorite (TTG) Magmas during Melting and Melt Segregation in the Continental Crust: Journal of Petrology, v. 50, n. 10, p. 1935, http://dx.doi.org/10.1093/petrology/egp060

Ghiorso, M. S., and Sack, R. O., 1995, Chemical mass transfer in magmatic processes IV. A revised and internally consistent thermodynamic model for the interpolation and extrapolation of liquid-solid equilibria in magmatic systems at elevated temperatures and pressures: Contributions to Mineralogy and Petrology, v. 119, n. 2–3, p. 197–212, http://dx.doi.org/10.1007/BF00307281

Grosfils, E. B., 2007, Magma reservoir failure on the terrestrial planets: Assessing the importance of gravitational loading in simple elastic models: Journal of Volcanology and Geothermal Research, v. 166, n. 2, p. 47–75, http://dx.doi.org/10.1016/j.jvolgeores.2007.06.007

Gutiérrez, F., and Parada, M. A., 2010, Numerical Modeling of Time-dependent Fluid Dynamics and Differentiation of a Shallow Basaltic Magma Chamber: Journal of Petrology, v. 51, n. 3, p. 731–762, http://dx.doi.org/10.1093/petrology/egp101

Henk, A., Franz, L., Teufel, S., and Oncken, O., 1997, Magmatic underplating, extension, and crustal reequilibration: Insights from a cross-section through the Ivrea zone and Strona-Ceneri 1zone, northern Italy: The Journal of Geology, v. 105, n. 3, p. 367–377, http://dx.doi.org/10.1086/515932

Hersum, T. G., Marsh, B. D., and Simon, A. C., 2007, Contact partial melting of granitic country rock, melt segregation, and re-injection as dikes into ferrar dolerite sills, McMurdo dry valleys, Antarctica: Journal of Petrology, v. 48, n. 11, p. 2125, http://dx.doi.org/10.1093/petrology/egm054

Hewitt, I. J., and Fowler, A. C., 2008, Partial melting in an upwelling mantle column: Proceedings of the Royal Society of London A, v. 464, n. 2097, p. 2467–2491, http://dx.doi.org/10.1098/rspa.2008.0045

Hildreth, W., and Moorbath, S., 1988, Crustal contributions to arc magmatism in the Andes of Central Chile: Contributions to Mineralogy and Petrology, v. 98, p. 455–489, http://dx.doi.org/10.1007/BF00372365

Hillert, M., 2007, Phase equilibria, phase diagrams, and phase transformations: their thermodynamic basis: Cambridge, Cambridge University Press, 526 p.

Hodge, D. S., 1974, Thermal model for origin of granitic batholiths: Nature, v. 251, p. 297–299, http://dx.doi.org/10.1038/251297a0
Holness, M. B., 2005, Spatial constraints on magma chamber replenishment events from textural observations of cumulates: the Rum Layered Intrusion, Scotland: Journal of Petrology, v. 46, n. 8, p. 1585, http://dx.doi.org/10.1093/petrology/egi027
Holness, M. B., and Winpenny, B., 2009, The Unit 12 allivalite, Eastern Layered Intrusion, Isle of Rum: a textural and geochemical study of an open-system magma chamber: Geological Magazine, v. 146, n. 3, p. 437, http://dx.doi.org/10.1017/S0016756808005797
Holness, M. B., Hallworth, M. A., Woods, A., and Sides, R. E., 2007, Infiltration metasomatism of cumulates by intrusive magma replenishment: the Wavy Horizon, Isle of Rum, Scotland: Journal of Petrology, v. 48, n. 3, p. 563, http://dx.doi.org/10.1093/petrology/egl072
Huppert, H. E., and Sparks, R. S. J., 1988, The generation of granitic magmas by intrusion of basalt into continental crust: Journal of Petrology, v. 29, n. 3, p. 599, http://dx.doi.org/10.1093/petrology/29.3.599
Irvine, T. N., 1974, Petrology of the Duke Island ultramafic complex, southeastern Alaska: GSA Memoirs, v. 138, p. 1–244, http://dx.doi.org/10.1130/MEM138-p1
——— 1980, Magmatic infiltration metasomatism, double-diffusive fractional crystallization, and adcumulus growth in the Muskox intrusion and other layered intrusions, *in* Hargraves, R. B., editor, Physics of Magmatic processes: Princeton, Princeton University Press, p. 325–384.
Jackson, M. D., and Cheadle, M. J., 1998, A continuum model for the transport of heat, mass and momentum in a deformable, multicomponent mush, undergoing solid-liquid phase change: International Journal of Heat and Mass Transfer, v. 41, n. 8–9, p. 1035–1048, http://dx.doi.org/10.1016/S0017-9310(97)00197-X
Jackson, M. D., Cheadle, M. J., and Atherton, M. P., 2003, Quantitative modeling of granitic melt generation and segregation in the continental crust: Journal of Geophysical Research-Solid Earth, v. 108, p. 2332, http://dx.doi.org/10.1029/2001JB001050
Jackson, M. D., Gallagher, K., Petford, N., and Cheadle, M. J., 2005, Towards a coupled physical and chemical model for tonalite–trondhjemite–granodiorite magma formation: Lithos, v. 79, n. 12, p. 43–60, http://dx.doi.org/10.1016/j.lithos.2004.05.004
Karlstrom, L., Dufek, J., and Manga, M., 2009, Organization of volcanic plumbing through magmatic lensing by magma chambers and volcanic loads: Journal of Geophysical Research, v. 114, B10204, http://dx.doi.org/10.1029/2009JB006339
——— 2010, Magma chamber stability in arc and continental crust: Journal of Volcanology and Geothermal Research, v. 190, n. 3–4, p. 249–270, http://dx.doi.org/10.1016/j.jvolgeores.2009.10.003
Katz, R. F., 2008, Magma dynamics with the enthalpy method: Benchmark solutions and magmatic focusing at mid-ocean ridges: Journal of Petrology, v. 49, n. 12, p. 2099–2121, http://dx.doi.org/10.1093/petrology/egn058
Katz, R. F., and Worster, M. G., 2008, Simulation of directional solidification, thermochemical convection, and chimney formation in a Hele-Shaw cell: Journal of Computational Physics, v. 227, n. 23, p. 9823–9840, http://dx.doi.org/10.1016/j.jcp.2008.06.039
Khazan, Y., 2010, Melt segregation and matrix compaction: the mush continuity equation, compaction/segregation time, implications: Geophysical Journal International, v. 183, n. 2, p. 601–610, http://dx.doi.org/10.1111/j.1365-246X.2010.04782.x
Langmuir, C. H., Bender, J. F., Bence, A. E., Hanson, S. R., and Taylor, G. N., 1977, Petrogenesis of basalts from the FAMOUS area: mid-Atlantic ridge: Earth and Planetary Science Letters, v. 36, n. 1, p. 133–156, http://dx.doi.org/10.1016/0012-821X(77)90194-7
Latypov, R. M., 2003, The origin of basic–ultrabasic sills with S-, D-, and I-shaped compositional profiles by *in-situ* crystallization of a single input of phenocryst-poor parental magma: Journal of Petrology, v. 44, n. 9, p. 1619–1656, http://dx.doi.org/10.1093/petrology/egg051
Le Bars, M., and Worster, M. G., 2006, Solidification of a binary alloy: Finite-element, single-domain simulation and new benchmark solutions: Journal of Computational Physics, v. 216, n. 1, p. 247–263, http://dx.doi.org/10.1016/j.jcp.2005.12.002
McKenzie, D., 1984, The generation and compaction of partially molten rock: Journal of Petrology, v. 25, n. 3, p. 713, http://dx.doi.org/10.1093/petrology/25.3.713
——— 1985, The extraction of magma from the crust and mantle: Earth and Planetary Science Letters, v. 74, n. 1, p. 81–91, http://dx.doi.org/10.1016/0012-821X(85)90168-2
——— 2011, Compaction and Crystallization in Magma Chambers: Towards a Model of the Skaergaard Intrusion: Journal of Petrology, v. 52, n. 5, p. 905–930, http://dx.doi.org/10.1093/petrology/egr009
Mei, S., Bai, W., Hiraga, T., and Kohlstedt, D. L., 2002, Influence of melt on the creep behavior of olivine-basalt aggregates under hydrous conditions: Earth and Planetary Science Letters, v. 201, n. 3–4, p. 491–507, http://dx.doi.org/10.1016/S0012-821X(02)00745-8
Morton, K. M., and Mayers, D. F., 1993, Numerical Solution of Partial Differential Equations: Cambridge, Cambridge University Press, 1345 p.
Nabelek, P. I., Hofmeister, A. M., and Whittington, A. G., 2012, The influence of temperature-dependent thermal diffusivity on the conductive cooling rates of plutons and temperature-time paths in contact aureoles: Earth and Planetary Science Letters, v. 317–318, p. 157–164, http://dx.doi.org/10.1016/j.epsl.2011.11.009
Naslund, H. R., and McBirney, A. R., 1996, Mechanisms of formation of igneous layering, *in* Cawthorn, R. G., editor, Layered Intrusions: The Netherlands, Amsterdam, Elsevier, p. 1–43.
Navon, O., and Stolper, E., 1987, Geochemical consequences of melt percolation: The upper mantle as a chromatographic column: The Journal of Geology, v. 95, n. 3, p. 285–307, http://dx.doi.org/10.1086/629131
Oertling, A. B., and Watts, R. G., 2004, Growth of and brine drainage from NaCl-H2O freezing: A simulation

of young sea ice: Journal of Geophysical Research-Oceans, v. 109, n. C4, http://dx.doi.org/10.1029/2001JC001109
Osborn E. F., and Tait, D. B., 1952, The system diopside-forsterite-anorthite: American Journal of Science, v. 250-A, p. 413–433.
Peressini, G., Quick, J. E., Sinigoi, S., Hofmann, A. W., and Fanning, M., 2007, Duration of a Large Mafic Intrusion and Heat Transfer in the Lower Crust: a SHRIMP U-Pb Zircon Study in the Ivrea-Verbano Zone (Western Alps, Italy): Journal of Petrology, v. 48, n. 6, p. 1185–1218, http://dx.doi.org/10.1093/petrology/egm014
Petford, N., 2003, Rheology of Granitic Magmas During Ascent and Emplacement: Annual Reviews of Earth and Planetary Sciences, v. 31, p. 399–427, http://dx.doi.org/10.1146/annurev.earth.31.100901.141352
Petford, N., and Gallagher, K., 2001, Partial melting of mafic (amphibolitic) lower crust by periodic influx of basaltic magma: Earth and Planetary Science Letters, v. 193, n. 3–4, p. 483, http://dx.doi.org/10.1016/S0012-821X(01)00481-2
Philpotts, A. R., Carroll, M., and Hill, J. M., 1996, Crystal-mush compaction and the origin of pegmatitic segregation sheets in a thick flood-basalt flow in the Mesozoic Hartford Basin, Connecticut: Journal of Petrology, v. 37, n. 4, p. 811–836, http://dx.doi.org/10.1093/petrology/37.4.811
Quick, J. E., Sinigoi, S., Negrini, L., Demarchi, G., and Mayer, A., 1992, Synmagmatic deformation in the underplated igneous complex of the Ivrea-Verbano zone: Geology, v. 20, n. 7, p. 613–616, http://dx.doi.org/10.1130/0091-7613(1992)020⟨0613:SDITUI⟩2.3.CO;2
Quick, J. E., Sinigoi, S., and Mayer, A., 1994, Emplacement dynamics of a large mafic intrusion in the lower crust of the Ivrea-Verbano Zone, northern Italy: Journal of Geophysical Research, v. 99, n. B11, p. 21,559–21,573, http://dx.doi.org/10.1029/94JB00113
——— 1995, Emplacement of mantle peridotite in the lower continental crust, Ivrea-Verbano zone, northwest Italy: Geology, v. 23, n. 8, p. 739–742, http://dx.doi.org/10.1130/0091-7613(1995)023⟨0739:EOMPIT⟩2.3.CO;2
Reiners, P. W., 1998, Reactive Melt Transport in the Mantle and Geochemical Signatures of Mantle-derived Magmas: Journal of Petrology, v. 39, n. 5, p. 1039–1061, http://dx.doi.org/10.1093/petroj/39.5.1039
Ribe, N. M., 1985, The generation and composition of partial melts in the earth's mantle: Earth and Planetary Science Letters, v. 73, n. 2–4, p. 361–376, http://dx.doi.org/10.1016/0012-821X(85)90084-6
Ricard, Y., Bercovici, D., and Schubert, G., 2001, A two-phase model for compaction and damage. 2. Applications to compaction, deformation and the role of interfacial surface tension: Journal of Geophysical Research-Solid Earth, v. 106, n. B5, p. 8907–8924, http://dx.doi.org/10.1029/2000JB900431
Richter, F. M., 1986, Simple models for trace element fractionation during melt segregation: Earth and Planetary Science Letters, v. 77, n. 3–4, p. 333–344, http://dx.doi.org/10.1016/0012-821X(86)90144-5
Richter, F. M., and McKenzie, D., 1984, Dynamical models for melt segregation from a deformable matrix: The Journal of Geology, v. 92, n. 6, p. 729–740, http://dx.doi.org/10.1086/628908
Rosenberg, C. L., and Handy, M. R., 2005, Experimental deformation of partially melted granite revisited: implications for the continental crust: Journal of Metamorphic Geology, v. 23, n. 1, p. 19, http://dx.doi.org/10.1111/j.1525-1314.2005.00555.x
Rushmer, T., and Jackson, M. D., 2006, Impact of melt segregation on tonalite-trondhjemite-granodiorite (TTG) petrogenesis: Transactions of the Royal Society of Edinburgh-Earth Sciences, v. 97, n. 4, p. 325–336, http://dx.doi.org/10.1017/S0263593300001486
Sawyer, E. W., 1991, Disequilibrium melting and the rate of melt-residuum separation during migmatization of mafic rocks from the Grenville Front, Quebec: Journal of Petrology, v. 32, n. 4, p. 701–738, http://dx.doi.org/10.1093/petrology/32.4.701
——— 1994, Melt segregation in the continental crust: Geology, v. 22, n. 11, p. 1019–1022, http://dx.doi.org/10.1130/0091-7613(1994)022⟨1019:MSITCC⟩2.3.CO;2
Schilling, J. G., and Winchester, J. W., 1969, Rare earth contribution to the origin of Hawaiian lavas: Contributions to Mineralogy and Petrology, v. 23, p. 27–37, http://dx.doi.org/10.1007/BF00371330
Schneider, M. C., and Beckermann, C., 1991, Effects of simplified enthalpy relations on the prediction of heat transfer during solidification of a lead-tin alloy: Applied Mathematical Modelling, v. 15, n. 11–12, p. 596–605, http://dx.doi.org/10.1016/S0307-904X(09)81005-6
Scott, D. R., and Stevenson, D. J., 1986, Magma ascent by porous flow: Journal of Geophysical Research-Solid Earth, v. 91, n. B9, p. 9283–9296, http://dx.doi.org/10.1029/JB091iB09p09283
Shamsundar, N., and Sparrow, E. M., 1975, Analysis of multidimensional conduction phase change via the enthalpy model: Journal of Heat Transfer, v. 97, n. 3, p. 333–340, http://dx.doi.org/10.1115/1.3450375
Shaw, D. M., 1970, Trace element fractionation during anatexis: Geochimica et Cosmochimica Acta, v. 34, n. 2, p. 237–243, http://dx.doi.org/10.1016/0016-7037(70)90009-8
——— 2000, Continuous (dynamic) melting theory revisited: Canadian Mineralogist, v. 38, n. 5, p. 1041–1063, http://dx.doi.org/10.2113/gscanmin.38.5.1041
Shirley, D. N., 1986, Compaction of igneous cumulates: The Journal of Geology, v. 94, n. 6, p. 795–809, http://dx.doi.org/10.1086/629088
Simpson, G., Spiegelman, M., and Weinstein, M. I., 2010, A multiscale model of partial melts: 1. Effective equations. Journal of Geophysical Research-Solid Earth, v. 115, B04410, http://dx.doi.org/10.1029/2009JB006375
Sinigoi, S., Quick, J. E., Mayer, A., and Demarchi, G., 1995, Density-controlled assimilation of underplated crust, Ivrea-Verbano Zone, Italy: Earth and Planetary Science Letters, v. 129, n. 1, p. 183–191, http://dx.doi.org/10.1016/0012-821X(94)00230-V
Sinigoi, S., Quick, J. E., Mayer, A., and Budahn, J., 1996, Influence of stretching and density contrasts on the chemical evolution of continental magmas: an example from the Ivrea-Verbano Zone: Contributions to Mineralogy and Petrology, v. 123, p. 238–250, http://dx.doi.org/10.1007/s004100050153

Solano, J. M. S., Jackson, M. D., Sparks, R. S. J., Blundy, J. D., and Annen, C., 2012, Melt Segregation in Deep Crustal Hot Zones: a Mechanism for Chemical Differentiation, Crustal Assimilation and the Formation of Evolved Magmas: Journal of Petrology, v. 53, n. 10, p. 1999–2026, http://dx.doi.org/10.1093/petrology/egs041

Sparks, D. W., and Parmentier, E. M., 1991, Melt extraction from the mantle beneath spreading centers: Earth and Planetary Science Letters, v. 105, n. 4, p. 368–377, http://dx.doi.org/10.1016/0012-821X(91)90178-K

Sparks, R. S. J., Huppert, H. E., Kerr, R. C., McKenzie, D. P., and Tait, S. R., 1985, Post-cumulus processes in layered intrusions: Geological Magazine, v. 122, n. 5, p. 555–568, http://dx.doi.org/10.1017/S0016756800035470

Spera, F. J., and Bohrson, W. A., 2001, Energy-constrained open-system magmatic processes I: General model and energy-constrained assimilation and fractional crystallization (EC-AFC) formulation: Journal of Petrology, v. 42, n. 5, p. 999–1018, http://dx.doi.org/10.1093/petrology/42.5.999

Spiegelman, M., 1993, Flow in deformable porous media. Part 1 Simple analysis: Journal of Fluid Mechanics, v. 247, p. 17–38, http://dx.doi.org/10.1017/S0022112093000369

——— 1996, Geochemical consequences of melt transport in 2-D: The sensitivity of trace elements to mantle dynamics: Earth and Planetary Science Letters, v. 139, n. 1–2, p. 115–132, http://dx.doi.org/10.1016/0012-821X(96)00008-8

Šrámek, O., Ricard, Y., and Bercovici, D., 2007, Simultaneous melting and compaction in deformable two-phase media: Geophysical Journal International, v. 168, n. 3, p. 964–982, http://dx.doi.org/10.1111/j.1365-246X.2006.03269.x

Tegner, C., Thy, P., Holness, M. B., Jakobsen, J. K., and Lesher, C. E., 2009, Differentiation and compaction in the Skaergaard intrusion: Journal of Petrology, v. 50, n. 5, p. 813, http://dx.doi.org/10.1093/petrology/egp020

Tharp, T. M., Loucks, R. R., and Sack, R. O., 1998, Modeling compaction of olivine cumulates in the Muskox Intrusion: American Journal of Science, v. 298, n. 9, p. 758–790, http://dx.doi.org/10.2475/ajs.298.9.758

van der Molen, I., and Paterson, M. S., 1979, Experimental deformation of partially melted granite: Contributions to Mineralogy and Petrology, v. 70, p. 299–318, http://dx.doi.org/10.1007/BF00375359

Vasilyev, O. V., Podladchikov, Y. Y., and Yuen, D. A., 1998, Modeling of compaction driven flow in poroviscoelastic medium using adaptive wavelet collocation method: Geophysical Research Letters, v. 25, n. 17, p. 3239–3242, http://dx.doi.org/10.1029/98GL52358

von Bargen, N., and Waff, H. S., 1986, Permeabilities, interfacial areas and curvatures of partially molten systems: Results of numerical computations of equilibrium microstructures: Journal of Geophysical Research-Solid Earth, v. 91, n. B9, p. 9261–9267, http://dx.doi.org/10.1029/JB091iB09p09261

Voschage, H., Hofmann, A. W., Mazzucchelli, M., Rivalenti, G., Sinigoi, S., Raczek, I., and Demarchi, G., 1990, Isotopic evidence from the Ivrea Zone for a hybrid lower crust formed by magmatic underplating: Nature, v. 347, p. 731–736, http://dx.doi.org/10.1038/347731a0

Wager, L. R., 1961, A note on the origin of ophitic texture in the chilled olivine gabbro of the Skaergard Intrusion: Geological Magazine, v. 98, n. 5, p. 353–366, http://dx.doi.org/10.1017/S0016756800060829

Walte, N. P., Bons, P. D., and Passchier, C. W., 2005, Deformation of melt-bearing systems—insight from *in-situ* grain-scale analogue experiments: Journal of Structural Geology, v. 27, n. 9, p. 1666–1679, http://dx.doi.org/10.1016/j.jsg.2005.05.006

Weill, D. F., Stebbins, J. F., Hon, R., and Carmichael, I. S. E., 1980, The enthalpy of fusion of anorthite: Contributions to Mineralogy and Petrology, v. 74, p. 95–102, http://dx.doi.org/10.1007/BF00375493

Whittington, A. G., Hofmeister, A. M., and Nabelek, P. I., 2009, Temperature-dependent thermal diffusivity of the Earth's crust and implications for magmatism: Nature, v. 458, n. 7236, p. 319–321, http://dx.doi.org/10.1038/nature07818

Williams, R. W., and Gill, J. B., 1989, Effects of partial melting on the uranium decay series: Geochimica et Cosmochimica Acta, v. 53, n. 7, p. 1607–1619, http://dx.doi.org/10.1016/0016-7037(89)90242-1

Wilson, J. R., Esbensen, K. H., and Thy, P., 1981, Igneous petrology of the synorogenic Fongen-Hyllingen layered basic complex, South-Central Scandinavian Caledonides: Journal of Petrology, v. 22, n. 4, p. 584–627, http://dx.doi.org/10.1093/petrology/22.4.584

Wolf, M. B., and Wyllie, P. J., 1991, Dehydration-melting of solid amphibolite at 10 kbar: Textural development, liquid interconnectivity and applications to the segregation of magmas: Mineralogy and Petrology, v. 44, n. 3, p. 151–179, http://dx.doi.org/10.1007/BF01166961

——— 1995, Liquid segregation parameters from amphibolite dehydration melting experiments: Journal of Geophysical Research-Solid Earth, v. 100, n. B8, p. 15,611–15,621, http://dx.doi.org/10.1029/95JB00660

Wood, B. J., and Blundy, J., 2003, Trace element partitioning, *in* Carlson, R. W., editor, The Mantle and Core: Treatise on Geochemistry, v. 2, p. 395–424, http://dx.doi.org/10.1016/B0-08-043751-6/02009-0

Zingg, A., 1990, The Ivrea crustal cross-section (northern Italy and southern Switzerland), *in* Salisbury M. H., and Fountain D. M., editors, Exposed Cross Sections of the Continental Crust: Dordrecht, The Netherlands, Kluwer, NATO ASI Series, v. 317, p. 1–19, http://dx.doi.org/10.1007/978-94-009-0675-4_1

Zou, H., 1998, Trace element fractionation during modal and nonmodal dynamic melting and open-system melting: A mathematical treatment: Geochimica et Cosmochimica Acta, v. 62, n. 11, p. 1937–1945, http://dx.doi.org/10.1016/S0016-7037(98)00115-X

——— 2000, Modeling of trace element fractionation during non-modal dynamic melting with linear variations in mineral/melt distribution coefficients: Geochimica et Cosmochimica Acta, v. 64, n. 6, p. 1095–1102, http://dx.doi.org/10.1016/S0016-7037(99)00383-X